Science of the Total Environment 650 (2019) 365–383

Contents lists available at ScienceDirect

Science of the Total Environment

journal homepage: www.elsevier.com/locate/scitotenv

Hydrological response of Chamelia watershed in Mahakali Basin to climate change

Vishnu Prasad Pandey *, Sanita Dhaubanjar, Luna Bharati, Bhesh Raj Thapa

International Water Management Institute (IWMI), Nepal Office, Lalitpur, Nepal

HIGHLIGHTS

- The first study evaluating spatio-temporal distribution in water availability to climate change in Chamelia.
- Maximum temperature under RCP scenarios and for three future periods are projected to increase in a range of 0.9-3.4°C).
- Streamflow is projected to increase gradually from near to far future under both RCPs, e.g. 12.2% in mid-future & RCP4.5

GRAPHICAL ABSTRACT

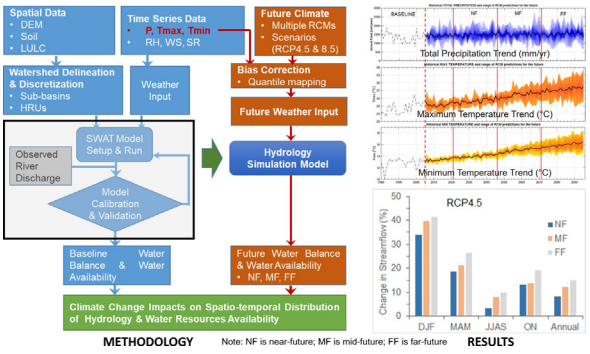

ARTICLE INFO

Article history:
Received 9 April 2018
Received in revised form 4 September 2018
Accepted 4 September 2018
Available online 5 September 2018

Editor: Ouyang Wei

Keywords:
Chamelia watershed
Climate change
Hydrological modeling
Mahakali
SWAT
Water resources

ABSTRACT

Chamelia (catchment area = 1603 km^2), a tributary of Mahakali, is a snow-fed watershed in Western Nepal. The watershed has 14 hydropower projects at various stages of development. This study simulated the current and future hydrological system of Chamelia using the Soil and Water Assessment Tool (SWAT). The model was calibrated for 2001–2007; validated for 2008–2013; and then applied to assess streamflow response to projected future climate scenarios. Multi-site calibration ensures that the model is capable of reproducing hydrological heterogeneity within the watershed. Current water balance above the Q120 hydrological station in the forms of precipitation, actual evapotranspiration (AET), and net water yield are 2469 mm, 381 mm and 1946 mm, respectively. Outputs of five Regional Climate Models (RCMs) under two representative concentration pathways (RCPs) for three future periods were considered for assessing climate change impacts. An ensemble of bias-corrected RCM projections showed that maximum temperature under RCP4.5 (RCP8.5) scenario for near-, mid-, and far-futures is projected to increase from the baseline by 0.9 °C (1.1 °C), 1.4 °C (2.1 °C), and 1.6 °C (3.4 °C), respectively. Minimum temperature for the same scenarios and future periods are projected to increase by 0.9 °C (1.2 °C), 1.6 °C (2.5 °C), and 2.0 °C (3.9 °C), respectively. Average annual precipitation under RCP4.5 (RCP8.5) scenario for near-, mid-, and far-futures are projected to increase by 10% (11%), 10% (15%), and 13% (15%), respectively. Based on the five RCMs considered, there is a high consensus for increase in temperature but higher uncertainty with respect to precipitations. Under these projected changes, average annual streamflow was simulated to increase gradually from the near to far future under both RCPs; for instance, by 8.2% in near-, 12.2% in mid-, and 15.0% in far-future under RCP4.5 scenarios. The results are useful for planning water infrastructure projects, in Chamelia and throughout the Mahakali basin, to ensure long-term sustainability under climate change.

* Corresponding author.
E-mail address: v.pandey@cgiar.org (V.P. Pandey).

https://doi.org/10.1016/j.scitotenv.2018.09.053
0048-9697/

1. Introduction

River basins across the globe are experiencing varying degrees of impacts from climate change (Kim and Kaluarachchi, 2009; Zhu and Ringler, 2012; Kure et al., 2013; Manandhar et al., 2013; Khadka et al., 2014; Shrestha and Htut, 2016; Versini et al., 2016; etc.). Snow-fed watersheds are considered even more vulnerable (Barnett et al., 2005; Immerzeel et al., 2013). The Intergovernmental Panel on Climate Change (IPCC), based on Coupled Model Intercomparison Project (CMIP5), has defined a series of Representative Concentration Pathways (RCP) for future climate projections (Van Vuuren et al., 2011). As per the RCP scenarios, temperature is projected to rise with high confidence and summer monsoon precipitation is projected to rise across South Asia with medium confidence (IPCC, 2013). These changes may alter the hydrologic systems (Bolch et al., 2012) leading to (but not limited to) disappearance of natural springs, loss or functional change in wetlands, increased variability in streamflow, and glacier retreat (Bates et al., 2008). This may consequently cause losses in transient groundwater storage (Andermann et al., 2012), agricultural productivity and yield, rural and urban livelihoods due to intermittent water supply, industrial productivity, and overall economy (Dixit et al., 2009; WECS, 2011; IWMI, 2014).

Water has been identified as the key resource for development and economic growth of Nepal (WECS, 2011). Because of possible impacts on future water availability and spatio-temporal distribution, climate change (CC) is frequently discussed in national development discourse in Nepal (Dixit et al., 2009). The climatic trends in Nepal reveal significant warming in recent decades (Devkota and Gyawali, 2015) and CC scenarios for Nepal across multiple general circulation models (GCMs) show considerable convergence on continued warming, with averaged mean temperature projected to increase by 1.2 °C and 3 °C by 2050 and 2100, respectively (World Bank, 2009). Studies in Nepalese basins such as Koshi have shown a large increase in intra- and inter-annual variability in climate and streamflows (Bharati et al., 2014, 2016). Another study (Manandhar et al., 2013) has shown that average annual and seasonal streamflows are expected to increase with a rise in temperature in the Kali Gandaki basin. As water is the crucial resource for socio-economic development of Nepal, it is imperative to understand likely impacts of CC on future water availability and incorporate them in future water resource planning. However, studies on projected future climate scenarios and associated impacts on spatio-temporal distributions and availability of water resources are limited, particularly in western Nepal. This study therefore considers evaluating climate change impacts on hydrological responses of Chamelia, a snow-fed tributary at the headwaters of Mahakali River Basin in Western Nepal (Fig. 1). This is the first study of this nature in the watershed, and it is important especially given the context of several planned hydropower projects.

The Mahakali basin, as delineated at a point (latitude = 28°28′42″; longitude = 80°31′38″) below the Nepal-India border in the Digo Jal Bikas Project, covers 17,377 km^2. Mahakali is a transboundary basin with about two-thirds of the basin falling in India and the rest in Nepal. The Mahakali river forms the border between India and Nepal and then joins Ganges basin in India (Fig. 1). Chamelia is the largest watershed in the Nepalese side of the Mahakali Basin, covering an area of 1603 km^2. Any intervention in the form of water infrastructure or management is expected to have impacts on downstream communities in both Nepal and India. Chamelia is also highly vulnerable to CC in comparison to other mid-hill watersheds in Nepal (Siddiqui et al., 2012). The watershed has been a center for hydropower development in recent

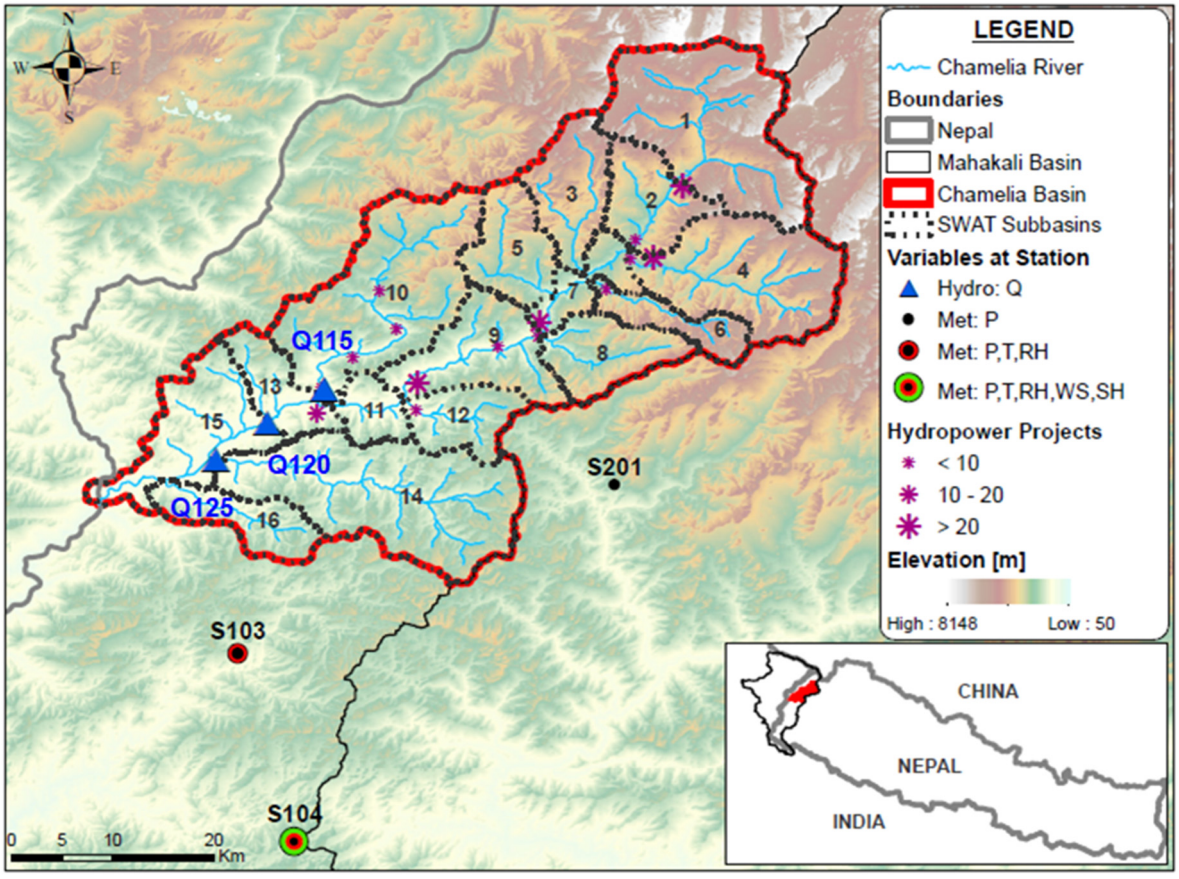

Fig. 1. Topography, river network, hydro-meteorological stations, and planned hydropower projects in Chamelia watershed. Inset shows location of Chamelia in western Nepal. "*" represents hydropower projects in various stages of development, with symbol size indicating production capacity of hydropower projects in megawatts (MW).

years. According to the data from Department of Electricity Development (DoED) Chamelia has 14 hydropower projects in various stages of development, with individual capacity ranging from 1 to 40 megawatts (MW), and a total capacity of 214 MW; 56.5 MW are either operational or under construction (IWMI, 2017). Some small-scale irrigation projects also exist in the watershed. CC may affect various aspects of such water infrastructure projects, all of which are manifested through hydrological alterations. Though CC is already experienced in the South Asian region (IPCC, 2013), no prior study has evaluated the extent of change and consequences on water availability in the Chamelia watershed. A quantification of spatial and temporal change in water availability across the basin is a key information to discuss implication of CC across the multiple sectors under the Nepalese water-energy-food nexus (Rasul, 2016).

This study aims to address this missing quantification of CC impacts on water availability in the Chamelia watershed, a tributary of Mahakali. We have three-fold objectives: i) to assess current spatio-temporal variations in water availability; ii) to project future temperature and rainfall; and iii) to assess the impacts of projected changes in temperature and rainfall on water availability. We simulate the current hydrology of Chamelia watershed using the Soil and Water Assessment Tool (SWAT); project future climate based on multiple Regional Circulation Models (RCMs); and then assess the response of the sub-watersheds to projected climate. Specifically, projected temperature and rainfall are generated using quantile mapping bias-correction of five RCM outputs. Change in climate and water availability is evaluated for three future periods: near-future (NF: 2021–2045), mid-future (MF: 2046–2070), and far-future (FF: 2071–2095), with respect to simulation for the baseline (1980–2005).

2. Methodology and data

Overall methodological framework adopted in this study is depicted in Fig. 2. Broadly, it consists of data preparation, model setup, model calibration and validation, current hydrological characterization, future climate projection, and CC impacts assessment on water availability using the validated SWAT model. The methodology is elaborated in the following sub-sections.

2.1. SWAT theory

SWAT is a process-based hydrological model that can predict impacts of climatic and non-climatic changes on water, sediment and agricultural chemical yields in complex basins with varying soils, land use/cover and management conditions (Arnold et al., 1998; Srinivasan et al., 1998). The main components of the model pertinent to hydrological analysis include: climate, hydrology, plant growth, land management, channel and reservoir routing.

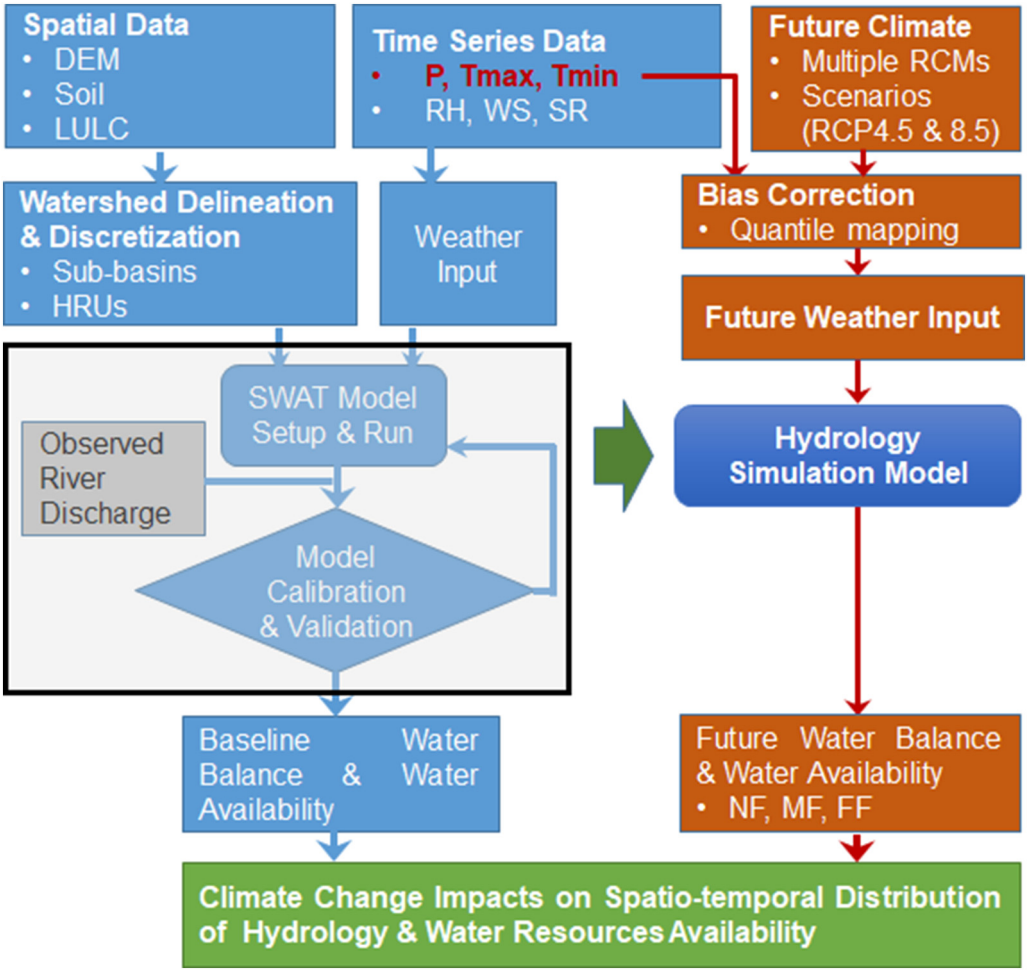

Fig. 2. Methodological framework adopted in this study. Blue indicates processes related to hydrological modeling while orange indicates processes related to climate projection and impacts. Both contribute to the end goal to evaluate climate change impacts shown in green. DEM is digital elevation model; LULC is land use/cover; P is precipitation; Tmax and Tmin are maximum and minimum temperatures; RH is relative humidity; WS is wind speed; SR is solar radiation; RCP is representative concentration pathways; RCMs is regional climate models; SWAT is soil and water assessment tool; NF is near-future; MF is mid-future; FF is far-future.

Conceptually, SWAT is semi-distributed and divides a basin into sub-basins. Each sub-basin is connected through a stream channel and further divided into Hydrologic Response Units (HRUs). HRU is a unique combination of a soil, land use/cover (LULC) and slope type in a sub-watershed. SWAT simulates hydrology, vegetation growth, and management practices at the HRU level. The hydrological processes explicitly modeled within each HRU are: soil water balance, surface runoff, infiltration, evapotranspiration (ET), canopy storage, plant uptake, percolation, return flow, recharge (shallow and deep aquifers), lateral flow, seepage, baseflow (from shallow aquifer) and groundwater pumping (Neitsch et al., 2011; Srinivasan, 2012). Since the model maintains a continuous water balance, the subdivision of the basin into unique HRUs, enables it to reflect differences in evapotranspiration for various LULCs and soils. Thus runoff is predicted separately for each sub-basin and routed to obtain the total runoff at the basin outlets. This provides a better physical description of the water balance. Detailed descriptions of the model can be found in Arnold et al. (1998), Srinivasan et al. (1998), and Neitsch et al. (2011).

2.2. Spatial data preparation

Three types of spatial data are required as input to SWAT model: digital elevation model (DEM), LULC, and soil type. Spatial distribution in topography in this study is represented by the Advanced Space borne Thermal Emission and Reflection Radiometer (ASTER) Global Digital Elevation Model Version 2 (GDEM V2) with 1-arc second resolution (approximately 30 m at the equator) (NASA JPL, 2009). ASTER GDEM, shown in Fig. 1, was jointly developed by the Ministry of Economy, Trade, and Industry (METI) of Japan and the United States National Aeronautics and Space Administration (NASA). A threshold area of 1000 ha was defined to create river network based on the ASTER DEM. As per the DEM, topography across the Chamelia watershed varies from 505 to 7090 m (Fig. 1).

The LULC in Fig. 3a is prepared based on a map from ICIMOD (2010). There are nine LULC types in the study area. Forest (40%) and rainfed agriculture (28%) are the dominant types accounting for more than two-thirds of the Chamelia watershed (Fig. 3a). Snow/glacier covers 6.3% of the watershed.

The soil type data is prepared based on the data developed by SOTER program (Dijkshoorn and Huting, 2009). There are seven types of soil in the watershed (Fig. 3b); the dominant among them are Eutric Regosols (23.8%), Eutric Cambisols (24.5%), and Gelic Cambisols (22.0%). The properties of each soil type are defined by hydraulic conductivity, appearance and depth.

2.3. Time series data preparation

There are no meteorological stations within the study watershed. Meteorological data from three stations close to the study watershed (Fig. 1) were obtained from the Department of Hydrology and Meteorology (DHM). Discharge data are available at three stations located within the catchment (Fig. 1). Rainfall and temperature data were formatted as per SWAT's input template and were used in the original units of mm and °C. SWAT requires daily relative humidity in fraction, however, two sets of observed data per day (morning and evening) were available in percentage. The average of the two data was taken and converted into fraction. SWAT requires solar radiation in MJ/m^2/day but observations are available in sunshine hours. The conversion from sunshine hours to solar radiation (MJ/m^2/day) was made using the Angstrom-Prescott (AP) model (Allen et al., 1998). SWAT requires wind speed in m/s, however, observed data were available in km/h. They were converted into m/s. All time-series data were quality checked for extent of missing values, typographic issues and coding errors. Overlaps in timeframes across all datasets were assessed to identify calibration and validation periods as periods with the best observed data.

2.4. SWAT model setup

ArcSWAT2012 was used as the interface to setup the model for Chamelia. To better represent heterogeneity, the watershed was discretized into 16 sub-watersheds as shown in Fig. 1. The watersheds were further discretized into 225 HRUs. The average size of the sub-watershed is 100.2 km^2, varying from 33.2 to 233.5 km^2. Multiple HRUs were defined using LULC (2%), soil type (5%) and slope (10%). Slopes for the purpose of defining HRUs were divided into four classes (0–3%; 3–15%; 15–30%; and >30%). Ten elevation bands, at intervals of 500 m, were defined to model the process of snowmelt and orographic distribution of temperature and precipitation. Weather input was fed in the form of daily rainfall (3 stations), maximum and minimum temperatures (2 stations), relative humidity (2 stations), wind speed (1 station) and sunshine hours (1 station) (Table 1). Daily time series of weather were used. SCS curve number method was used to estimate surface runoff, where daily curve number is estimated based on a function of soil moisture. The Penman-Monteith method was used to estimate potential evapotranspiration (PET). Variable storage method was applied to route flow in the channels. No point discharge was defined.

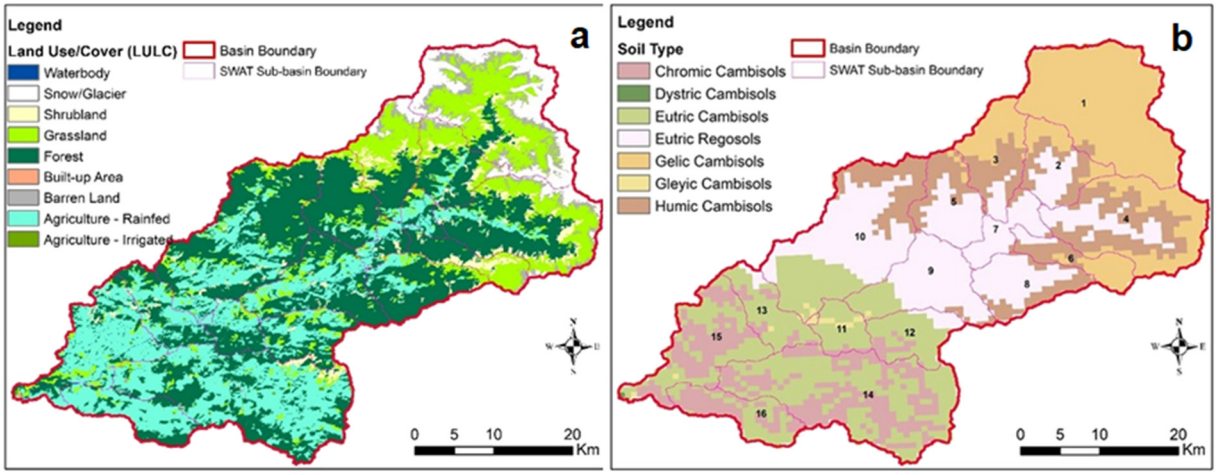

Fig. 3. Spatial distribution in – a) land use/cover, and soil type (b) – within Chamelia.

Table 1
Description of hydro-meteorological data used in this study.

Index	Lat.	Lon.	Elevation (masl)	S. name	River	Drainage (km^2)	Variables	Duration
115	29.702	86.607	784	Harsing Bagar	Naugraha Gad	203	Q	2001–2013
120	29.672	80.558	724	Karkale Gaon	Chamelia River	1150	Q	2001–2013
125	29.638	80.514	580	Panjewanya	Jamari Gad	228	Q	2001–2009
103	29.467	80.533	1266	Patan (West)	–	–	P, T, RH	2001–2013
104	29.300	80.583	1848	Dadeldhura	–	–	All	2001–2013
201	29.617	80.867	1456	Pipalkot	–	–	P	2001–2013

Note: masl is "meters above mean sea level"; Index is "station number of Department of Hydrology and Meteorology, Nepal"; Lat. Is "latitude"; Lon. Is "longitude"; S. is "station"; Q is "river discharge"; P is "precipitation"; T is "temperature"; RH is "relative humidity"; all means all five meteorological variables (P, T, RH, sunshine hours, and wind speed).

2.5. Model calibration and validation

Calibration is the parameterization of a model to a given set of conditions, thereby reducing the prediction uncertainty (Arnold et al., 2012). SWAT model for Chamelia watershed was calibrated and validated at three hydrological stations (Table 1; Fig. 1) with daily observed streamflow data. The multi-site calibration approaches are considered as better one against the single site calibration as demonstrated in Hasan and Pradhanang (2017). The hydrological data at the three stations were evaluated using exploratory analysis tools such as hydrographs, mass curves, and data reading. Data availability varied at each station so periods with consistent and good quality data with no or negligible missing data were identified for each station independently. At stations Q120 and Q115, timeframe of 2001–2013 was selected with calibration and validation periods of 2001–2007 and 2008–2013, respectively. At Q125, 2001–2009 was selected with calibration and validation periods of 2001–2005 and 2006–2009, respectively. A warm up period of 3 years was used to develop appropriate soil and groundwater conditions before calibration (Fontaine et al., 2002). The model was calibrated in three stages: i) Sensitivity analysis, ii) Auto-calibration in SWAT-CUP, and iii) manual calibration. Sensitivity was analysed using global sensitivity approach, wherein, one parameter value is changed at a time while keeping others constant. Auto-calibration was run for 1000 iterations with parameter ranges recommended in SWAT documentations (Neitsch et al., 2011). Although the range of values for the sensitive parameters was narrowed down during auto-calibration, the simulated and observed hydrographs did not match well. Then manual calibration was performed on the results of the auto-calibration by tweaking relevant model parameters to match the simulated hydrograph to the observed.

During manual calibration, adjustments were initially made to the most sensitive parameters and then to the less sensitive ones. Parameters other than those identified during the sensitivity analysis were also adjusted for more realistic values leading to better performance of the model. Visual inspection of the hydrographs (peaks, time to peak, shape of the hydrograph and baseflow); scattered plots; flow duration curve; statistical parameters; and water balance comparison (observed verses simulated) at daily, monthly and annual scales were used as the basis for evaluating model performance. Following statistical parameters were considered for performance evaluation: coefficient of determination (R^2), Nash-Sutcliffe efficiency (NSE), percent bias (PBIAS), and change in mean values. Details of these methods are available in Nash and Sutcliffe (1970), Gupta et al. (1999), and Moriasi et al. (2007). The model performance was evaluated for both monthly and daily simulations. Due care was given to keep physically based parameters within a reasonable range (Table 4) throughout the calibration process.

2.6. Uncertainty assessment

Predictive uncertainty was assessed using SUFI-2 algorithm (Abbaspour et al., 2007), which defines uncertainty as the discrepancy between measured and simulated variables. The predictive uncertainties reflect all sources of uncertainty, i.e. conceptual model, forcing inputs (e.g. rainfall), and parameter (Rostamian et al., 2008). The uncertainty of input parameters in SUFI-2 is depicted as a uniform distribution, while model output uncertainty is quantified using 95% prediction uncertainty (95PPU) band and associated measures (i.e., p-factor and r-factor). The p-factor is the percentage of data bracketed in the 95PPU band and measures the portion of uncertainty the model is capturing. The r-factor, calculated as a ratio of mean width of the 95PPU band and standard deviation, on the other hand, captures the goodness of calibration; smaller the 95PPU band better the calibration result. The 95PPU plot, p-factor and r-factor were obtained using SWAT-CUP.

2.7. Future climate projections

The IPCC represent possible futures in the form of representative concentration pathways (RCPs). Four RCP pathways are developed for the climate modeling community as a basis for long-term and near-term modeling experiments. They are RCP2.6, RCP4.5, RCP6.0, and RCP8.5 (Van Vuuren et al., 2011). It is the innovative collaboration between integrated assessment modelers, climate modelers, terrestrial ecosystem modelers and emission inventory experts. RCM outputs are generally only available for RCP4.5 and 8.5 and occasionally for RCP2.6. In this study, RCP4.5 is selected as a medium stabilizing scenario and RCP8.5 as a very high emission scenario. RCP4.5 refers to stabilization without overshoot pathway leading to 4.5 W/m^2 (~650 ppm CO_2) at stabilization after 2100; where as RCP8.5 refers to rising radiative forcing pathways leading to 8.5 W/m^2 (~1370 ppm CO_2) by 2100.

Outputs from five RCMs (Table 2) were used in this study as representative future climates. They are combinations of four unique Global Circulation Models (GCMs) downscaled dynamically by three unique RCMs. Three CCAM models and one REMO model were selected based on review of past studies in South Asia (Saeed and Suleri, 2015; Li et al., 2016; Mukherjee et al., 2017). Additionally, the ICHEC-RCA4 model was selected as it showed closest correspondence to observed precipitation in rigorous assessment of the past performance of 11 RCMs for in the Hindu Kush Himalayas carried out by Ghimire et al. (2015). The five RCMs and their un-weighted average ensemble were used as future climate inputs. Using such multi-model ensembles can reduce the overall uncertainty in model predictions (Scinocca et al., 2015). Precipitation data from ICHEC-RCA4 and REMO were in $kg/m^2/s$ unit, which were converted into millimeters (mm) before further use. For RCMs with 365-day calendars, an additional day in leap years was filled with data from the preceding day. RCM gridded data were processed using the Climate Data Operators (CDO). Future climate time series (daily precipitation and min/max temperature) were extracted from these RCMs at the three meteorological stations.

Bias correction of raw RCM outputs is highly recommended for hydrological applications, especially for applications at finer spatial scales (Teutschbein and Seibert, 2012; Wilby, 2010; Wood et al., 2004). A paper comparing multiple bias correction methods considering outputs of multiple RCMs for Western Nepal undertaken by the authors is under development. Quantile mapping (QM) has emerged as a better technique for bias correction for improving the past performance of RCMs

Table 2
Description of RCMs considered in this study.

SN	Unique name	CORDEX South Asia RCM	RCM description (source)	Contributing CORDEX modeling center	Driving GCM	Calendar	Unit: P [T]
1	ACCESS_CCAM	CSIRO-CCAM-1391 M	ConformalCubi Atmospheric Model - CCAM (McGregor and Dix, 2001)	Commonwealth Scientific and Industrial Research Organisation (CSIRO)	ACCESS1.0	365 days	mm [K]
2	CNRM_CCAM	CSIRO-CCAM-1391 M	ConformalCubi Atmospheric Model - CCAM (McGregor and Dix, 2001)	Commonwealth Scientific and Industrial Research Organisation (CSIRO)	CNRM-CM5	365 days	mm [K]
3	MPI.ESM_CCAM	CSIRO-CCAM-1391 M	ConformalCubi Atmospheric Model - CCAM (McGregor and Dix, 2001)	Commonwealth Scientific and Industrial Research Organisation (CSIRO)	MPI-ESM-LR	365 days	mm [K]
4	MPI.E.MPI_REMO	MPI-CSC-REMO2009	MPI Regional model 2009 (Teichmann et al., 2013)	Climate Service Center (CSC), Germany	MPI-ESM-LR	366 days	kg/m^2/s [K]
5	ICHEC_RCA4	SMHI-RCA4	Rossby Centre regional atmospheric model version 4 -RCA4 (Samuelsson et al., 2011)	Rossby Centre, Swedish Meteorological and Hydrological Institute (SMHI), Sweden	ICHEC-EC-EARTH	366 days	kg/m^2/s [K]

Note: P is precipitation; T is temperature; RCM is regional circulation model; GCM is Global Circulation Model; CORDEX is coordinated regional climate downscaling experiment.

(Berg et al., 2012; Chen et al., 2013; Lutz et al., 2016; Teutschbein and Seibert, 2012). This study considers future climate data at three meteorological stations bias-corrected using QM method (Gudmundsson et al., 2012).

QM corrects quantiles of raw RCM data to match with that of observed ones using transfer functions. When the distribution is expected to change (i.e., more extreme rainfall events, change in wet/dry days), extra complexity is warranted in bias-correction, and so the choice of QM is necessary at finer (e.g., daily) resolutions (Shrestha et al., 2017a, b). Both distribution-based and empirical QM are used in correcting precipitation and temperature. In this study, empirical QM was implemented in R using Gudmundsson et al.'s (2012) qmap package, where regularly spaces quantiles are approximated by linear functions.

2.8. Climate change impact assessment

The calibrated and validated SWAT model was forced with the bias corrected projections for daily precipitation and temperatures (maximum and minimum). Simulations of futures were undertaken based on five RCM outputs as well their ensemble. The ensemble inputs were prepared by taking an average of the five selected RCMs for each daily time step. Studies comparing past-performance of RCMs for the South Asian domain find that multi-modal ensembles often perform better than individual RCMs with lower biases and standard deviations (Choudhary and Dimri, 2017; Ghimire et al., 2015; Sanjay et al., 2017). IPCC reports (Knutti et al., 2010a; Knutti et al., 2010b; Wilby, 2010) also encourage thoughtful usage of multi-modal ensembles.

With two RCPs and five RCMs and an ensemble, 12 different future scenarios were generated and run in the SWAT model. The simulated streamflows based on the future projection were then synthesized in terms of long-term annual average and seasonal values for the three future periods: near-future (2021–2045), mid-future (2046–2070), and far-future (2071–2095). Finally, change in streamflow at annual and seasonal scales with respect to simulated baseline values are reported as an impact of CC on water resources availability. To characterize spatial variation, change in sub-basin level values of key water balance components is also shown.

2.9. Data and sources

Spatial and time-series data reflecting biophysical, hydro-climatic and future climatic contexts required in this study were collected from local and global sources. Information related to existing and planned water infrastructures within the watershed were obtained from literature. The details of data required by SWAT, their description, and sources are provided in Table 3 below.

3. Results and discussion

3.1. Hydrological model development

A hydrological model for Chamelia was set up, calibrated and validated in SWAT. Model parameters related to runoff, evapotranspiration, groundwater and soil water were adjusted to represent observed hydrological patterns at the three hydrological stations shown in Fig. 1.

Table 3
Data and sources used in this study.

Dataset [unit]	Data type	Data description/properties	Data source	Resolution (time frame)
Terrain [m]	Spatial grids	Digital elevation model (DEM)	NASA JPL (2009)	30 m × 30 m grids (for 2009)
Soil [–]	Spatial vectors	Soil classification and physical properties (e.g., texture, porosity, field capacity, wilting point, saturated conductivity and soil depth)	Dijkshoorn and Huting (2009)	1:1 million map (from multiple years)
Land use/cover (LULC) [–]	Spatial grids	Landsat land use/cover classification (9 classes)	ICIMOD (2010)	30 m × 30 m grids (for 2010)
Precipitation [mm]	Time-series	Daily observed precipitation	Department of Hydrology and Meteorology (DHM), Nepal	3 stations (2001–2013)
Temperature [°C]	Time-series	Daily observed minimum and maximum temperature	DHM, Nepal	2 stations (2001–2013)
Relative humidity [–]	Time-series	Daily observed mean relative humidity	DHM, Nepal	2 stations (2001–2013)
Sunshine hours [h]	Time-series	Daily observed sunshine hours	DHM, Nepal	1 stations (2001–2013)
Wind speed [m/s]	Time-series	Daily observed mean wind speed	DHM, Nepal	1 stations (2001–2013)
River discharge [m^3/s]	Time-series	Daily observed streamflow	DHM, Nepal	3 stations (2001–2013)
Future precipitation [mm]	Time-series extracted from spatial grids	Daily projected values	5 Regional Climate Models detailed in Table 2	0.44° × 0.44° (1970–2100)
Temperature [°C]				

The calibrated parameters are shown in Table 4. Sensitive parameters were not consistent throughout the sub-watersheds. However, the runoff curve number (CN2), groundwater delay (GW_DELAY) and baseflow recession factor (ALPHA_BF) were among the most sensitive parameters at all three stations, albeit with varying levels of influence.

The default values of SWAT parameters underestimated the baseflow in most cases. Therefore, CN2, one of the sensitive parameters that plays a key role in increasing the infiltration and subsequently the groundwater contribution to baseflow, was fine-tuned. The value of ALPHA_BF, which affects the shape of the receding limb of hydrograph, was changed based on visual assessment of the slope of the receding limb. Similarly, other flow related parameters such as soil evaporation compensation factor (ESCO), threshold depth of water in the shallow aquifer to trigger return flow (GWQMN), soil depth (SOL_Z), available water capacity of the soil (SOL_AWC), saturated hydraulic conductivity (SOL_K), effective hydraulic conductivity in main channel (CH_K2), lateral flow travel time (LATTIME), and channel Manning's number (CH_N2), among others, were adjusted to not only match the simulated and observed flows at daily and monthly scale but also to reasonably approximate the water balance components. Defining elevation bands allowed for variable temperature laps rate (TLAPS), which played an important role in replicating the spatial distribution of temperature, as seen in other studies as well (e.g., Rahman et al., 2012).

3.1.1. Model performance

Results show a good agreement between the simulated and observed streamflow values at all the three hydrological stations for both calibration and validation periods (Figs. 4–6). The model simulates reasonably well the hydrological regime for daily as well as monthly flows, reproducing flow duration curve (FDC), and keeping statistical parameters within reasonable range (Figs. 4–6) as discussed in Liu and de Smedt (2004) and Moriasi et al. (2007). Additionally, the hydrological response pattern follows the rainfall pattern at all the stations, for both daily and monthly simulations. As can be expected monthly simulation has better performance compared to daily. Difference between observed and simulated average annual values for calibration, validation and overall (calibration + validation) periods are <15% at all three stations (Table 5). Based on the general performance ratings

Table 4
Calibrated SWAT parameters at three hydrological stations (in decreasing order of sensitivity).

Station (river)	Parameter	Definition	Unit	Process (data file)[a]	Level[a]	Recommended range	Default value	Calibrated value
Karkale Gaon (Chamelia), Q120	CN2	SCS runoff curve number for moisture condition II	–	Runoff (.mgt)	HRU	35–98	Varies	1.2 (ratio)
	CANMX	Maximum canopy storage	mm	Runoff (.hru)	HRU	0–100	0	98
	CH_N1	Manning's "n" value for the tributary channel	–	Runoff (.sub)	Sub-basin	0.01–30	0.014	0.5
	ESCO	Soil evaporation compensation factor	–	Evaporation (.hru)	HRU	0–1	0.95	0.2
	GW_DELAY	Delay time for aquifer recharge	days	Groundwater (.gw)	HRU	0–500	31	5
	CH_N2	Manning's "n" value for the main channel	–	Channel (.rte)	Reach	0–1	0.014	0.15
	CH_K2	Effectivity hydraulic conductivity in main channel alluvium	mm/h	Channel (.rte)	Reach	0–500	0	300
	TLAPS	Temperature lapse rate	°C/km	Topographic effect (.sub)	Sub-basin	−10–10	−5.6	−7.9
	ALPHA_BF	Baseflow recession constant	days	Groundwater (.gw)	HRU	0–1	0.048	0.25
	LAT_TTIME	Lateral flow travel time	days	HRU (.hru)	HRU	0–180	0	80
	SOL_K	Saturated soil conductivity	mm/h	Soil (.sol)	HRU	0–2000	Varies	0.2 (ratio)
	SOL_Z	Depth from soil surface to bottom of layer	mm	Soil (.sol)	HRU	0–3500	Varies	2 (ratio)
Harsing Bagar (Naugraha Gad), Q115	CN2	SCS runoff curve number for moisture condition II	–	Runoff (.mgt)	HRU	35–98	Varies	1.15 (ratio)
	ESCO	Soil evaporation compensation factor	–	Evaporation (.hru)	HRU	0–1	0.95	0.4
	CH_K2	Effectivity hydraulic conductivity in main channel alluvium	mm/h	Channel (.rte)	Reach	0–500	0	450
	ALPHA_BF	Baseflow recession constant	days	Groundwater (.gw)	HRU	0–1	0.048	0.2
	CH_N2	Manning's "n" value for the main channel	–	Channel (.rte)	Reach	0–1	0.014	0.2
	TLAPS	Temperature lapse rate	°C/km	Topographic effect (.sub)	Sub-basin	−10–10	−5.6	−9.5
	LAT_TTIME	Lateral flow travel time	days	HRU (.hru)	HRU	0–180	0	30
	SOL_K	Saturated soil conductivity	mm/h	Soil (.sol)	HRU	0–2000	Varies	0.5 (ratio)
	SOL_AWC	Available water storage capacity of the soil layer	–	Soil (.sol)	HRU	0–1	Varies	0.5 (ratio)
	SOL_Z	Depth from soil surface to bottom of layer	mm	Soil (.sol)	HRU	0–3500	Varies	2.0 (ratio)
	GW_DELAY	Delay time for aquifer recharge	days	Groundwater (.gw)	HRU	0–500	31	90
	CANMX	Maximum canopy storage	mm	Runoff (.hru)	HRU	0–100	0	80
	EPCO	Plant uptake compensation factor	–	Evaporation (.hru)	HRU	0–1	1	0.6
	OV_N	Manning's n value for overland flow	–	HRU (.hru)	HRU	0.01–30	Varies	0.16 (ratio)
Panjewanya (Gamari Gad), Q125	GW_DELAY	Delay time for aquifer recharge	days	Groundwater (.gw)	HRU	0–500	31	60
	TLAPS	Temperature lapse rate	°C/km	Topographic effect (.sub)	Sub-basin	−10–10	−5.6	0
	SOL_Z	Depth from soil surface to bottom of layer	mm	Soil (.sol)	HRU	0–3500	Varies	2.0 (ratio)
	GWQMN	Threshold depth of water in shallow aquifer to occur groundwater return flow	mm	Soil (.gw)	HRU	0–5000	1000	4900
	ESCO	Soil evaporation compensation factor	–	Evaporation (.hru)	HRU	0–1	0.95	0.99
	CN2	SCS runoff curve number for moisture condition II	–	Runoff (.mgt)	HRU	35–98	Varies	0.98 (ratio)
	CH_K2	Effectivity hydraulic conductivity in main channel alluvium	mm/h	Channel (.rte)	Reach	0–500	0	450
	ALPHA_BF	Baseflow recession constant	days	Groundwater (.gw)	HRU	0–1	0.048	0.2
	LAT_TTIME	Lateral flow travel time	days	HRU (.hru)	HRU	0–180	0	40
	SOL_K	Saturated soil conductivity	mm/h	Soil (.sol)	HRU	0–2000	Varies	0.15 (Ratio)
	CH_N2	Manning's "n" value for the main channel	–	Channel (.rte)	Reach	0–1	0.014	0.15
	EPCO	Plant uptake compensation factor	–	Evaporation (.hru)	HRU	0–1	1	0.2
	SHALLST	Initial depth of water in shallow aquifer	mm	Groundwater (.gw)	HRU	0–50,000	1000	300

[a] For detailed explanation of the parameters, please refer to Arnold et al. (2012). Recommended and default values are as per SWAT documentation (Neitsch et al., 2011).

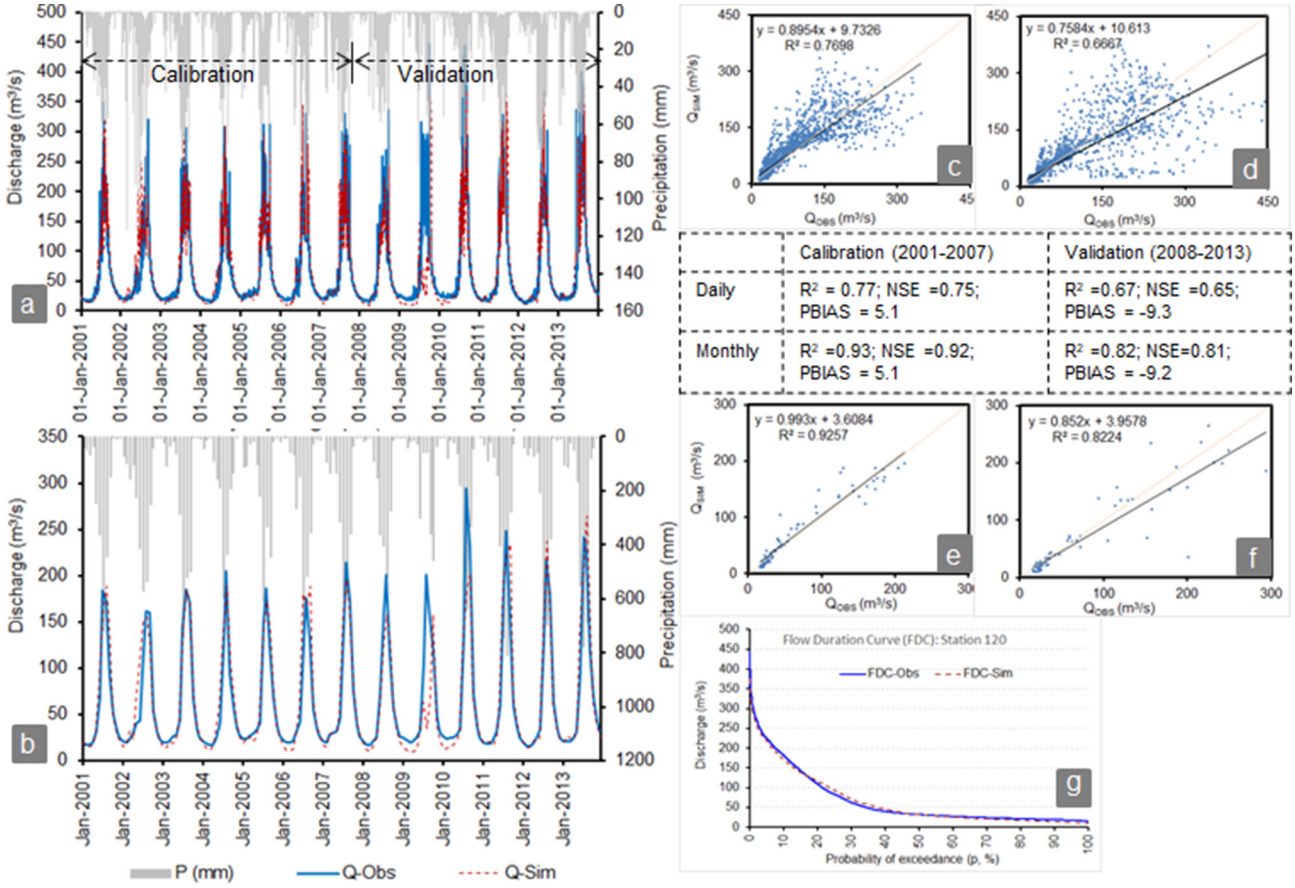

Fig. 4. Comparison of observed versus simulated stream flows at Karkalegaon (Index = Q120; River = Chamelia) station: a) Hydrograph for daily simulation, b) hydrograph for monthly simulation, c & d) scattered plots for daily calibration and validation, e & f) scattered plots for monthly flow calibration and validation, g) flow duration curve (FDC, daily).

criteria developed by Moriasi et al. (2007), for both monthly and daily time steps, model calibration results are "very good (NSE > 0.65)" for the stations Q120 and Q115 and "adequate (NSE = 0.54 to 0.65)" for the station Q125. For the validation period, the daily and monthly NSE range between 0.33 to 0.65 and 0.68 to 0.81 across the three stations, with relatively poorer performance at Q115.

A closer look into the hydrograph and scatter plots during calibration indicates that the model estimates low flows and long-term average reasonably well for both daily and monthly simulations. However, the scatter points are spread out further for high flows indicating that the model is poorer at simulating high peaks (or high flows). The equation of the linear fit shows that model is under-estimating flow at both daily and monthly scale. During validation, the scatter plot shows higher spread even for average-flows indicating that the model performance is poor for both high-flows as well as average flows even if low flow is reasonably reproduced. Overall, the model is better suited for low-flows estimation and water resources assessment and needs further calibration for use in flood-forecasting and extreme analysis. As the goal of this modeling is to assess water availability and its distribution in the long run, the model is considered adequate to serve the purpose.

Observed variation in performance across the hydrological stations can partly be attributed to limitations in the hydro-meteorological inputs. Studies have identified spatial variability in errors in rainfall, streamflow, soils map, and land use/cover inputs caused by various reasons, including poor sampling strategies. In this study, none of the selected meteorological stations lie directly inside Chamelia watershed. To account for variation in topography among the meteorological stations and within Chamelia watershed, values of meteorological variables were distributed spatially and topographically by assigning elevation bands in SWAT. Ten elevation bands, at intervals of 500 m, were defined to model the process of snowmelt and orographic distribution of temperature and precipitation. Of the three hydrological stations, st120 lies on the main stem of Chamelia, covering most of the watershed, and shows the best performance. Stations st115 and st125, on the other hand, are 1st order tributaries and drain smaller sub-watersheds within Chamelia. Therefore, streamflows generated at these stations will be more sensitive to errors in meteorological inputs, contributing to the poorer model performance.

In addition, accurate information on the snow and glaciers, coverage area, depth, and depletion rate is not available for the high altitude areas in the watershed. Considering potential uncertainties and limitations in the input data, the performance of the model in calibration and validation can be considered acceptable to simulate streamflow in the watershed. As seen in Fig. 1, most licensed hydropower projects lie upstream of the st120 station. The "very good" model performance at this station is key for assessment of impact due to these projects. Multi-site calibration (at three hydrological stations) assures that the model is capable of reproducing hydrological heterogeneity within the Chamelia watershed with higher reliability at stations of greater importance.

3.1.2. Predictive uncertainty of the model

Uncertainty is an inherent part of hydrological modeling (Latif, 2011) due to input data, model structure, and model parameters, among others (Leta et al., 2015). Exploratory data analysis was used to help reduce uncertainties in input data. This study adopted SUFI-2 algorithm, plotted 95PPU band, and then quantified the predictive uncertainty using p-factor and r-factor as described in Abbaspour et al. (2007). Other studies such as Rostamian et al. (2008), Shrestha et al.

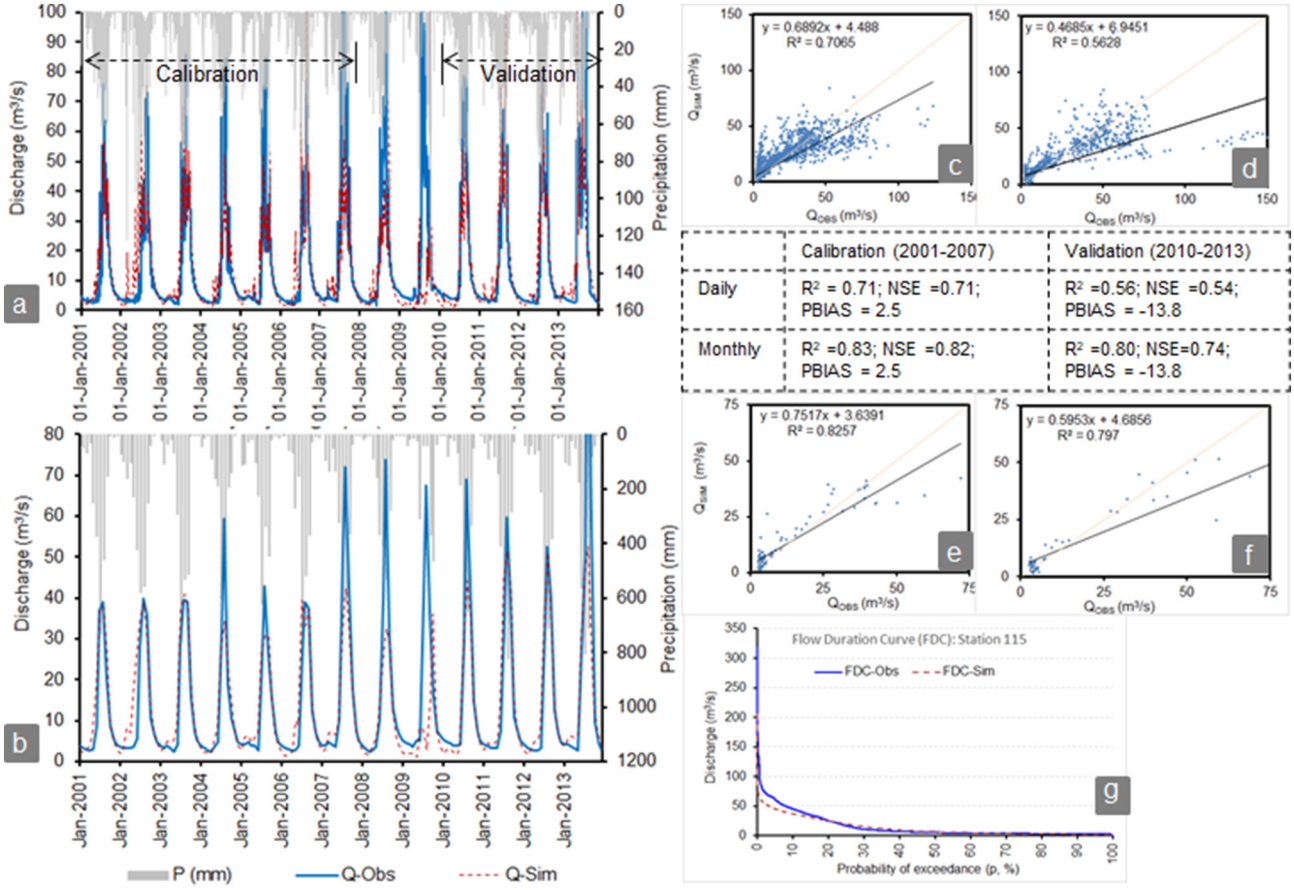

Fig. 5. Comparison of observed versus simulated stream flows at Harsing Bazar (Index = Q115; River = Naugraha Gad) station: a) Hydrograph for daily simulation, b) hydrograph for monthly simulation, c & d) scattered plots for daily calibration and validation, e & f) scattered plots for monthly flow calibration and validation, g) flow duration curve (FDC, daily).

(2017a), Shrestha et al. (2017b) and Krishnan et al. (2018) have also used similar approach. The ideal model would have a p-factor approaching to 100%, i.e. all observed data fall within the 95PPU band, and r-factor approaching to zero, i.e. predictive uncertainty is less than variability in observed data. Generally, higher p-factor can be obtained with an increased r-factor as wider bandwidths are more flexible to capture observed variations. But higher bandwidth indicates higher predictive uncertainties. The r-factor of less than one generally indicates a good calibration (Rostamian et al., 2008).

The daily hydrographs with 95PPU bands for all the three stations are shown in Annex-1. The 95PPU band is widest for Q120 with majority of the observations covered. At stations Q115 and Q125, the 95PPU bands are much narrower specially for high flow period. Both the p- and r-factors for the calibration at Q120 (catchment = 1150 km^2) were 0.91 and 0.79, respectively. It means 91% of the observed data points are within the 95PPU simulation bands and therefore the model predictions capture observations well. Similarly, for Q115 (catchment = 203 km^2), the p- and r-factors are 0.76 and 0.52. For Q125 (catchment = 228 km^2), p- and r-factors are 0.68 and 0.46, respectively. While Q115 and Q125 have lower prediction uncertainties than Q120, their ability to simulate observed data is low. Overall at the three stations (Q115, Q120, and Q125), the r-factor is in a range of 0.46–0.79 and p-factor in a range of 0.68–0.91. The model is therefore considered well calibrated and reasonably captures uncertainties.

More aggressive methods for disaggregating and quantifying the contribution of various sources (structure, parameter, input) towards total predictive uncertainty exist (Saltelli et al., 2006). However, all input datasets have limitations due to data availability quality, length and resolution. Observed hydro-meteorological data for Chamelia is only of acceptable quality for 12 years and none of the meteorological stations used are physically within the basin as shown in Fig. 1. Spatial data sets are coarse, often remotely based with limited field based verification. Hence input data uncertainty is potentially larger than parameter uncertainty. The lack of longer and higher quality observed datasets is a key barrier that did not provide a sufficient basis for a more rigorous analysis of propagation of input errors in the model and subsequent evaluation of model structure and parameter uncertainty. Hence only the standard SUFI-2 approach was used here to evaluate total predictive uncertainty.

3.2. Characterization of current hydrology

Current hydrology of the Chamelia watershed was characterized using simulated results from the SWAT model developed in this study. Four major hydrological components were considered for the analysis, namely, precipitation, actual evapotranspiration (ET), net water yield and the change in storage (Δ storage). The 'Δ storage' is a collective term including groundwater recharge, change in soil moisture storage in the vadose zone and other transmission losses in the system. Net water yield is the streamflow generated at the sub-basin outlet. Streamflow is the sum of surface runoff, lateral flow, and groundwater flow, with deductions for losses and abstractions.

Annual average precipitation, actual ET and net water yield of the basin at Q120 station for the simulation period (2001–2013) were 2469 mm, 381 mm and 1946 mm, respectively. The values, however, vary within each sub-basin (Fig. 7; please refer Fig. 1 for the sub-basins location). There is spatial heterogeneity in all the water balance components (Fig. 7). Net water yield shows a minimum value of

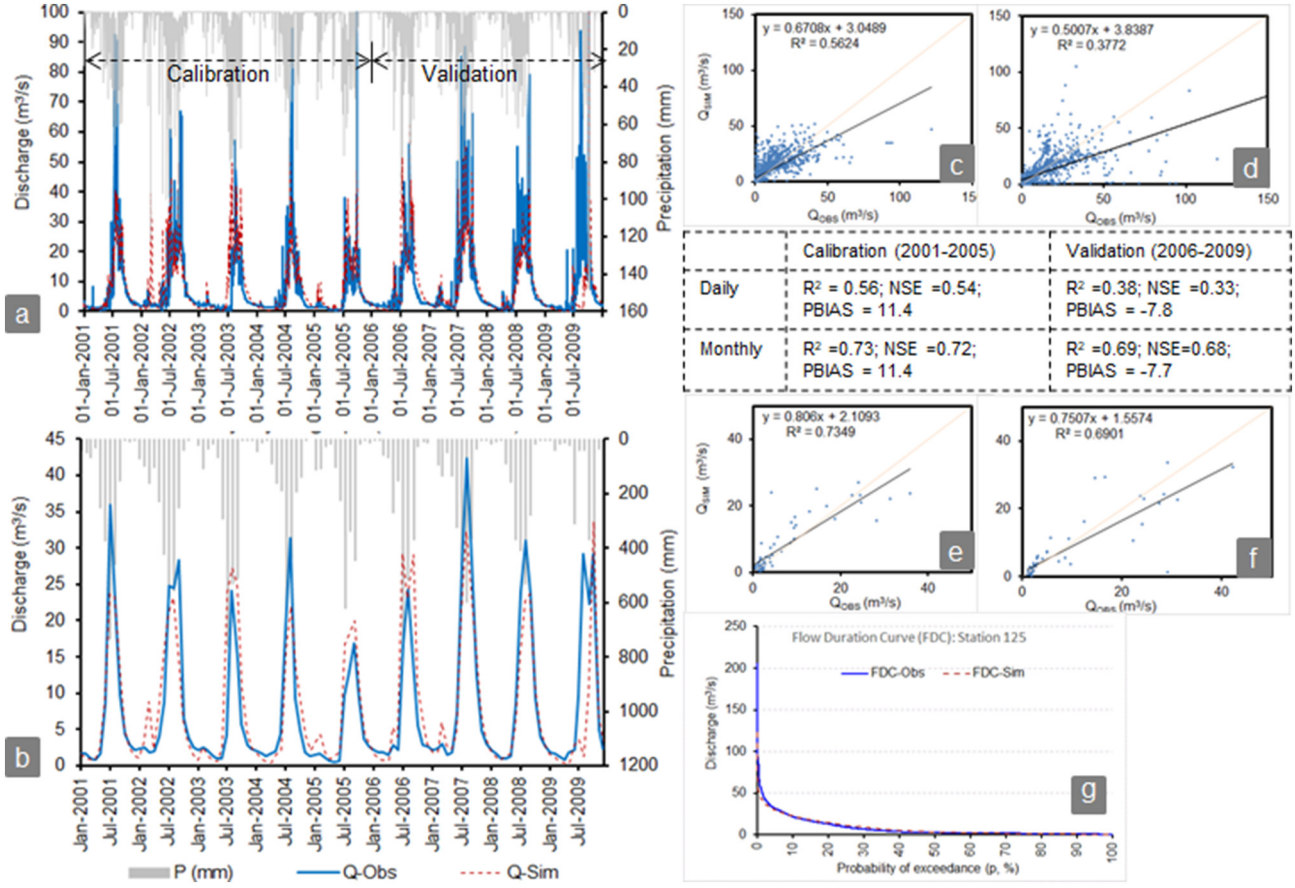

Fig. 6. Comparison of observed versus simulated stream flows at Panjewanya (Index = Q125; River = Jamari Gad) station: a) Hydrograph for daily simulation, b) hydrograph for monthly simulation, c & d) scattered plots for daily calibration and validation, e & f) scattered plots for monthly flow calibration and validation, g) flow duration curve (FDC, daily).

589 mm in the sub-basin 16, a tributary joining Chamelia near the outlet of the watershed and the maximum of 2152 mm in sub-basin 6, a tributary joining Chamelia near headwaters of the watershed (see Fig. 1 for sub-basin locations). Net water yield is greater than actual ET in most of the sub-basins in the upstream, represented by low sub-basin numbers. Low ET is reasonable as these sub-basins lie at higher elevations with low temperature. As ET depends largely on precipitation, land use/cover and temperature, it was estimated higher in forested areas. In case of actual ET, sub-basin 1 has the minimum value of 9 mm and sub-basin 11 has the highest values of 766 mm. Precipitation contributes to storage only in upstream basins in steep terrain while in downstream basins, storage contributes a baseflow. This indicates that aquifer recharge is largely happening in the hills. Furthermore, watersheds with more snow cover in upstream showed lower contribution of baseflow than other watersheds, which is consistent with literatures (e.g., Hasan and Pradhanang, 2017). On the other hand, watersheds in the downstream show more contribution from baseflow, which is likely due to interflow of water infiltrated in the upstream. These discussions indicate that the hydrological characteristics simulated by the model are reasonable.

Additionally, Fig. 8 shows a large temporal variation in the water balance components in the Chamelia watershed. Net water yield and actual ET are highest in the monsoon season and lowest in the dry season, as expected. 'Δ storage' is negative in monsoon with −134.5 mm in July (the wettest month) indicating recharge and positive in the dry season with 43.5 mm in December indicating groundwater contribution to streamflow. Relatively large value of the 'Δ storage' in monsoon season could be attributed to high groundwater recharge, which ultimately yields to high groundwater contribution to streamflow during the dry periods.

Table 5
Comparison of mean and standard deviations of observed and simulated average annual streamflows.

Station index	Period	Mean streamflow (m^3/s)			Standard deviation (m^3/s)		
		Obs.	Sim.	% Diff.	Obs.	Sim.	Diff.
st115	Calibration	13.29	13.63	2.6	2.5	1.7	−0.8
	Validation	17.55	15.13	−13.8	4.8	2.1	−2.7
	Overall	15.11	13.46	−10.9	3.6	2.6	−1.0
st120	Calibration	62.12	65.3	5.1	4.8	2.9	−1.9
	Validation	70.94	64.39	−9.2	7.0	6.0	−1.0
	Overall	66.19	64.88	−2.0	7.3	10.5	3.2
st125	Calibration	6.84	7.62	11.4	1.8	1.2	−0.6
	Validation	9.05	8.35	−7.7	2.0	2.1	0.1
	Overall	7.82	7.95	1.7	2.1	1.6	−0.5

Notes: Obs. is observed; Sim. is simulated; Diff. is difference.

3.3. Future climate projection

Raw projections extracted from the five selected RCMs for historical baseline (1980–2005) are presented in Annex-2. The raw data for both maximum and minimum temperatures showed under-estimation throughout the year. In case of maximum temperature, there was slight over-estimation for the moths of March, April, May and June. In case of precipitation, the raw RCM data showed over-estimation for most of the months, except February, March, and April (Annex-2. B). The raw RCM

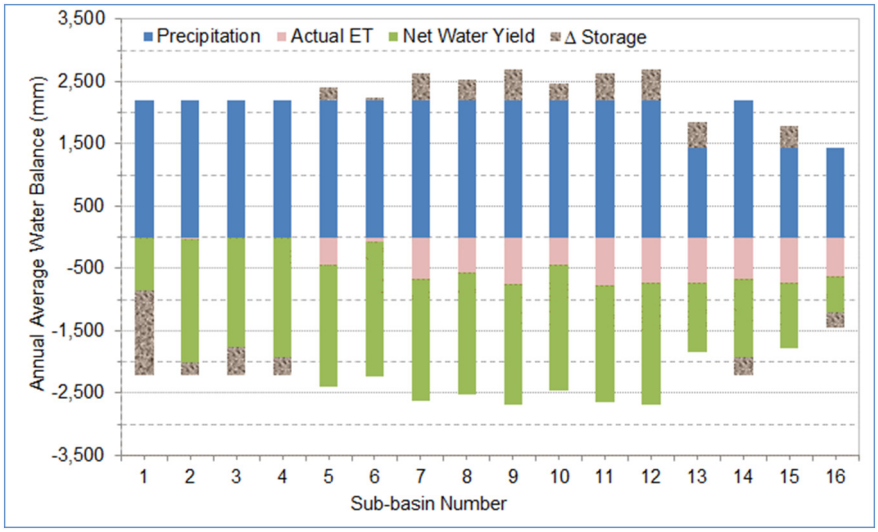

Fig. 7. Sub-basin wise long-term annual average water balance from SWAT model simulations (2001–2013) in Chamelia. See Fig. 1 for location of sub-basin within the watershed, low numbers represent upstream basins. ET is evapotranspiration.

daily projections were bias-corrected using quantile-mapping method to remove seen biases. The statistical parameters before and after bias-correction at climate station st103 are shown in Annex-3. Comparative plots and performance statistics show that R^2 is improved to a great extent by bias correction. For ensemble outputs as an example, R^2 values have increased from −1.67 to 0.65 for precipitation, from 0.37 to 0.90 for maximum temperature, and from 0.59 to 0.95 for minimum temperature. Other statistical indicators have also improved to a reasonable level after bias correction (Annex-3).

Projected precipitation and min/max temperature extracted at the three selected meteorological stations from five RCMs (Table 3) under RCP4.5 and RCP8.5 scenarios were bias-corrected. Three future timeframes were considered: near future (NF, 2021–2045), mid-future (MF, 2046–2070), and far-future (FF, 2071–2095). The period of 1980–2005 was considered as climate baseline. The future climate projections are discussed here are based on the downscaled RCM values at a meteorological station (Index = 103) because of proximity to the watershed.

3.3.1. Projected precipitation

Annual total precipitation for the climate baseline and future periods show no obvious trend (Fig. 9). Projected range of annual total precipitation for the three future periods are 1080–1732 (NF); 821–2560 mm (MF); and 670–1743 mm (FF); respectively. It indicates an increase in the uncertainty range when we progress further with the future.

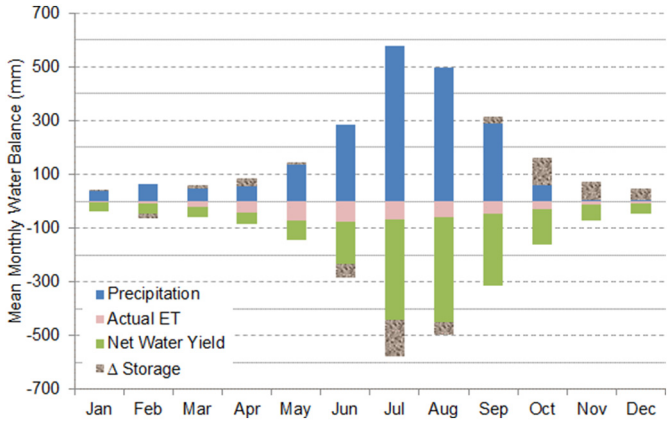

Fig. 8. Mean monthly water balance from model simulation (2001–2013) in Chamelia watershed. ET is evapotranspiration.

The range of changes in projected total precipitation by the five RCMs is presented in Fig. 10. It is clear that the annual ranges are not representative of the seasonal changes as the negative and positive changes across the seasons are averaged out in the annual values. As can be expected, the three CCAM models based on the same dynamic downscaling show similar behaviours and ranges. Studies have shown that precipitation trends in RCMs are dominated by the driving RCMs rather than the driving GCMs in South Asia (ul Hasson, 2016). ICHEC_RCA4 shows high spread in predictions with wet bias while the REMO model appears to predict drier conditions. This is in line with finding from Ghimire et al. (2015), where South Asian RCMs show positive wet bias for mid elevations. However, the medians for most cases in Fig. 10 lie within the ±50% range, suggesting that the RCMs predict increase in annual precipitation for some years and decrease in others. For these cases, medians (line in the box plot) and the means (x in the box plot) lie close to each other and close to the 0 line for the pre-monsoon and monsoon months. Such a lack of skewness in data indicates that increase and decrease in precipitation are projected equally across the years for DJF, MAM, JJAS. For post-monsoon months (ON), medians lie below the means indicating the projections are negatively skewed.

Considering the range of predictions as a measure of uncertainty, the annual and monsoon (JJAS) precipitations show the least uncertainty. Post-monsoon (ON) precipitation shows the high level of uncertainty for all the scenarios and futures considered. Even the projections by different RCMs do not vary much for the annual and monsoon season projections but vary significantly for other seasons. The higher prediction range indicates a more erratic behaviour of rainfall and its intensity at a seasonal scale. It should be additionally noted that the use of three CCAM-based models is bound to highlight the trends seen in CCAM model as more likely. A higher number and variety of RCMs would allow for an objective discussion of uncertainty and consensus in predictions seen across RCMs.

Table 6 summarizes the projected changes in average annual and seasonal precipitation values for RCP4.5 and RCP 8.5 scenarios based on the ensemble of five RCMs. Average annual values are projected to increase consistently over three future periods, however, the rate of change varies over the years (Table 6). Taking an example of RCP4.5 scenarios, average annual precipitation is projected to increase by 10% in NF and 13% in FF; however, it varies over the years from −10 to 30%

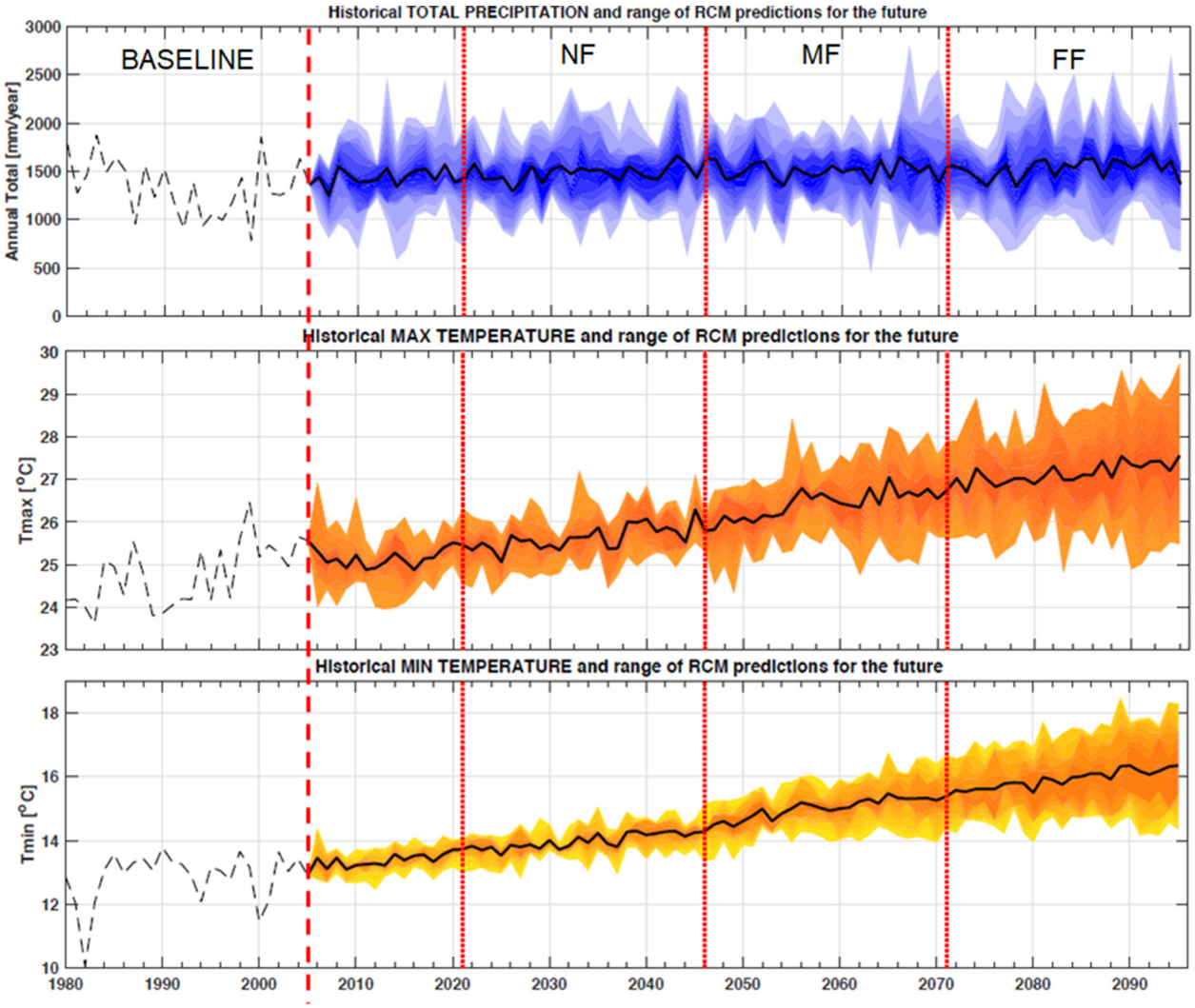

Fig. 9. Trends in long-term average annual total precipitation and max/min temperature at station 103. Baseline period shows observed data while future timeframes show range of bias-corrected projections from different RCMs for both RCP scenarios. NF, MF and FF refer to near-, mid- and far-futures, respectively. The dark line shows ensemble of the 5 RCMs for the two scenarios. Shaded areas indicate range in the projections.

for NF and − 5 to 34% for FF. The rate of increase is even higher for RCP8.5 scenarios.

We further analysed whether the annual increase applies to all the seasons. Table 6 shows that only MAM season follows consistent increasing trends from NF to FF as the case of annual values; albeit, the rate of change is higher for MAM season compared to the annual ones. Other seasons do not show a consistent gradual increasing or decreasing trends from NF to FF; however, all the seasons show an increasing trend from NF to MF. The range of projection bracket increases when we move from NF to MF, suggesting again for higher degree of uncertainly in projection when we move towards far future.

Such trends suggest that the RCMs show consensus that future change will likely increase amount of winter rain (from westerlies) and extend the duration. The two rainfall seasons typically seen in Western Nepal are likely to be more prominent under climate change.

The dry season ensemble values indicate increasing trend, however decreasing trend is also projected by some of RCMs. In addition, the magnitude and direction of change is not consistent through the years and RCMs. The average increasing trend in precipitation gives a reflection of positive impacts. This potential increase can help hydropower developers generate more energy during dry season; contribute to overcoming energy-scarcity; and provide water for dry season irrigation. In the meantime, as the demand for dry season energy is higher, it promises more revenue to the hydropower developers. However, increased rainfall may aggravate water-induced disasters such as landslides and floods (Bajracharya et al., 2018), especially downstream of the river system. This may result in land degradation and ultimately impact on lives and livelihoods of the people who are less climate resilient.

3.3.2. Projected temperature

Unlike precipitation, average annual time series of the projected temperature shows a clear increasing trend until the end of the century for both maximum and minimum temperatures (Fig. 9). Projected range of average annual maximum temperature within each future periods are 25.5–27.1 °C for NF, 25.6–27.1 °C for MF, and 25.5–29.7 °C for FF (Fig. 9), higher than the baseline value of 24.1 °C. In case of minimum temperature, the range is 12.8–14.4 °C for NF, 13.7–14.7 for MF, and 14.4–18.3 for FF. In both cases, the range widens when we move further towards future, reflecting more uncertainty towards far future.

3.3.2.1. Maximum temperature. The range of predictions for maximum temperature across the different RCM provides more consensus and certainty than that seen for precipitation. All changes for all RCMs, RCPs and futures indicate increase with both means and medians

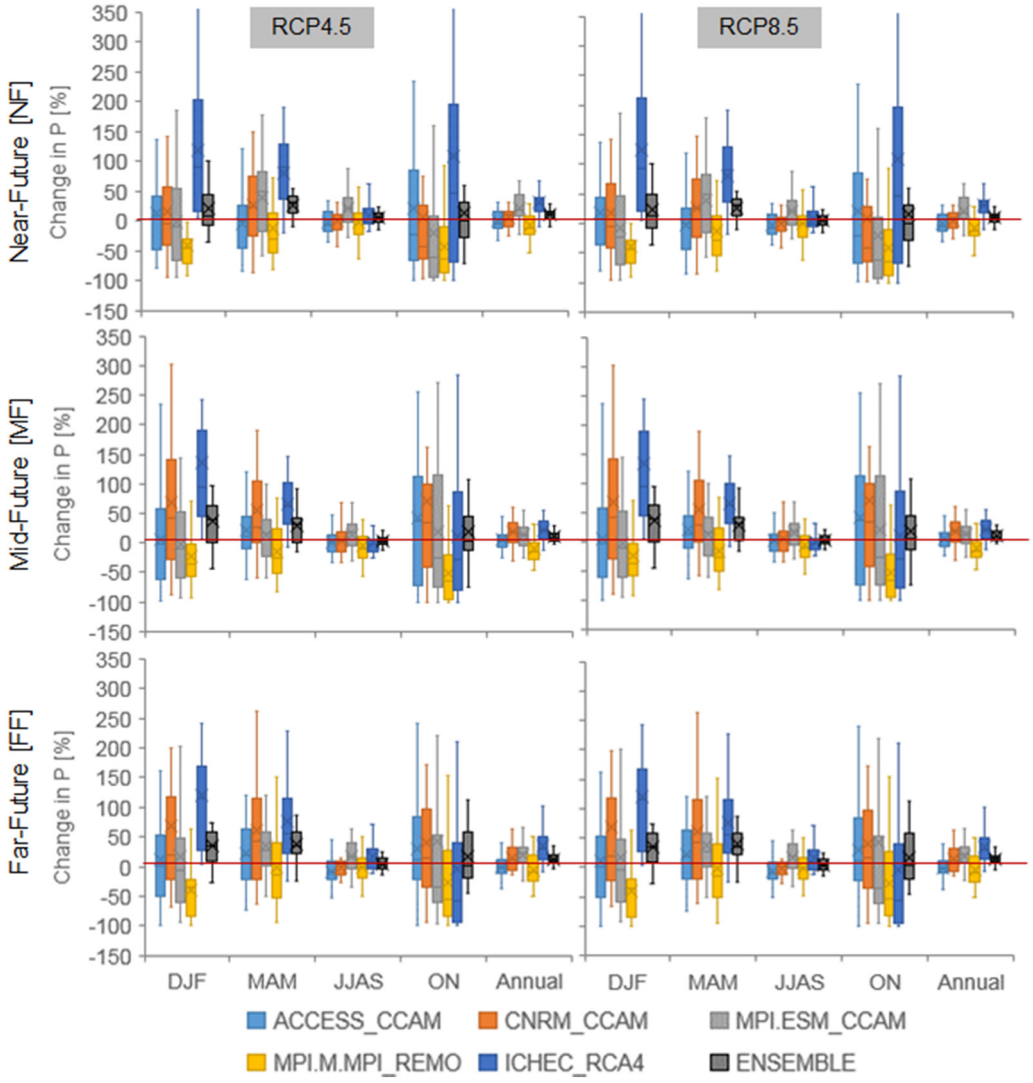

Fig. 10. Range of projected change in annual total future precipitation for different futures, RCPs and RCMs at station 103. Each box represents range in one RCM where whiskers indicate max and min values excluding the outliers, line markers indicate the median and x markers indicate the mean of change in annual total precipitation projected for each future timeframe. (Notes: DJF is December–January–February (winter season); MAM is Mach–April–May (dry season); JJAS is June–July–August–September (rainy/monsoon season); ON is October–November (post-monsoon season).)

Table 6
Projected changes in total precipitation [mm] at seasonal and annual scales at st103 station based on an ensemble of five RCMs under RCP scenarios.

Change from baseline [%]			DJF	MAM	JJAS	ON	Annual
Baseline [mm]			111.8	206.0	982.5	39.3	1340.7
RCP 4.5	NF	Mean [%]	22	26	5	15	10
		Range [%]	−36–162	−33–90	−14–24	−72–341	−10–30
	MF	Mean [%]	37	28	3	18	10
		Range [%]	−45–209	−15–92	−13–22	−74–208	−3–29
	FF	Mean [%]	35	39	5	16	13
		Range [%]	−28–134	−25–86	−14–24	−46–113	−5–34
RCP 8.5	NF	Mean [%]	22	29	6	18	11
		Range [%]	−35–75	−27–90	−11–30	−52–180	−5–27
	MF	Mean [%]	13	38	11	12	15
		Range [%]	−38–106	2–120	−12–36	−52–104	−2–35
	FF	Mean [%]	16	44	8	42	15
		Range [%]	−37–99	−7–122	−20–26	−40–197	−13–31

Notes: DJF is December–January–February (winter season); MAM is Mach–April–May (dry season); JJAS is June–July–August–September (rainy/monsoon season); ON is October–November (post-monsoon season).

lying above zero (Fig. 11). The mean and median overlaps for all cases indicating the projections over the years are spread evenly above and below the mean. It is interesting to note that despite the disparity in projected precipitation across ICHEC_RCA4 and REMO model, the maximum temperature (and minimum as well) follow the same behaviour with overlapping ranges. On the other hand, the three CCAM models are slightly dissimilar in comparison to their behaviour for precipitation.

Projected average annual maximum temperature for RCP4.5 scenarios, based on an ensemble of five RCMs, are gradually increasing compared to the baseline over three future periods by 0.9 °C (for NF), 1.4 °C (for MF) and 1.6 °C (for FF) (Table 7). In case of RCP8.5, it is projected to increase by 3.4 °C until the FF. It is increasing across all the seasons too, but the amount of increase is not consistent. Winter (DJF) temperature is projected to increase more for all the three futures and two scenarios considered, followed by dry (or pre-monsoon; MAM) season (Table 7). It reflects that warmer winters are expected in the Chamelia watershed during all the future periods considered. However, it should be noted that rate of increase is not consistent throughout the RCMs and years as shown as range in Table 7. The range of uncertainty in the

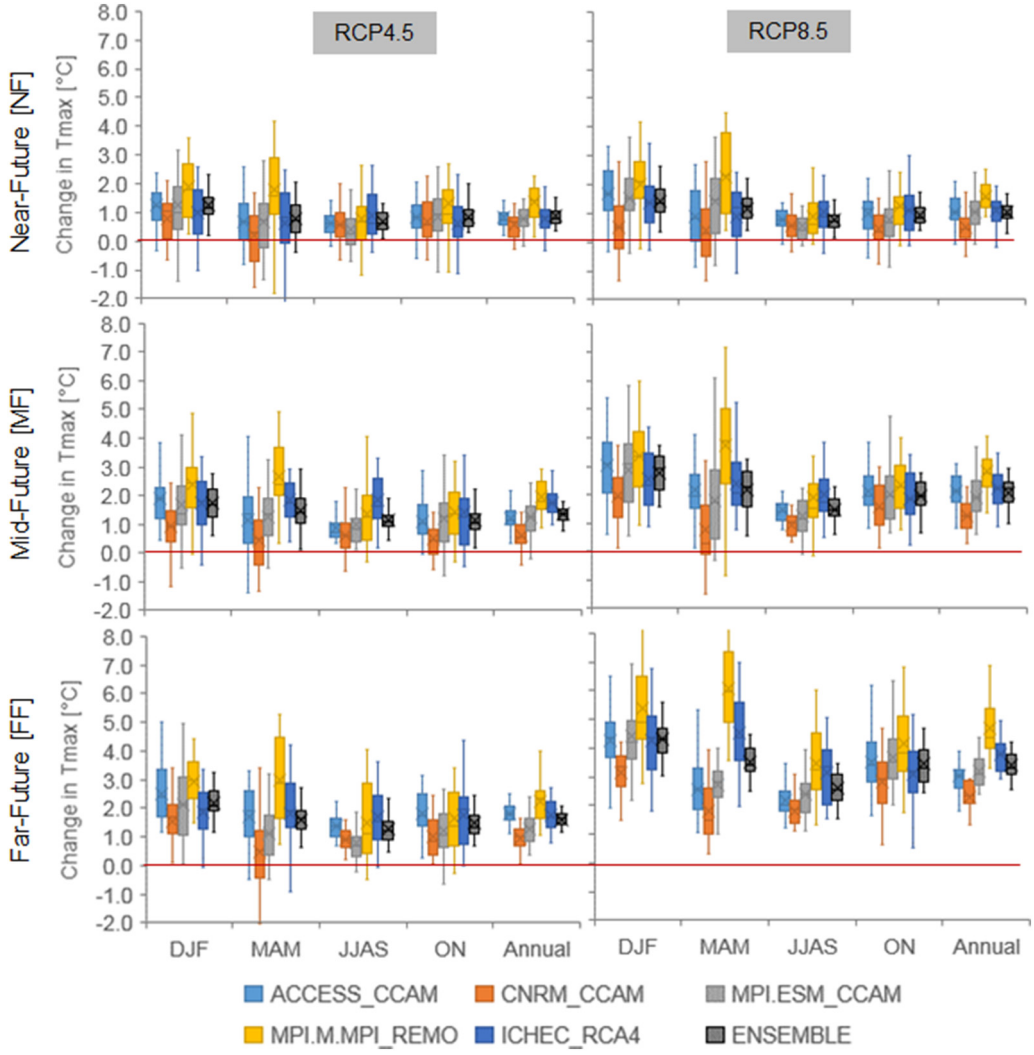

Fig. 11. Range of projected change in future maximum temperature for different scenarios and RCMs for the study watershed. Each box represents range in one RCM where whiskers indicate max and min values excluding the outliers, line markers indicate the median and x markers indicate the mean of change in annual total precipitation projected for each future timeframe.

projection is relatively high in winter (DJF) and pre-monsoon (MAM) seasons (Fig. 11).

3.3.2.2. Minimum temperature. The range of predictions for minimum temperature across the different RCMs, RCPs, and seasons provide more consensus and certainty that future minimum temperatures will rise as all model medians and majority of model projections lie above zero (Fig. 12).

The average annual minimum temperature is projected to increase from the baseline value by 0.9 °C, 1.7 °C, and 2.0 °C for NF, MF and FF, respectively, under RCP4.5 scenarios (Table 8). In case of RCP8.5 scenarios, the rate of increase is significantly higher; up to 3.9 °C increase from the baseline period for FF. The increasing trend is consistent across all the seasons and for both the scenarios; albeit the rate of increase varies with the season. A higher rate of increase is projected for summer (JJAS) and winter (DJF) seasons in both scenarios, which means warmer nights in the summer and winter. The uncertainty range in the change of projected minimum temperature varies with season; higher degree of uncertainty exists in pre- and post-monsoon seasons (Fig. 12). Unlike precipitation, the range of uncertainty in temperature increase (both minimum and maximum) is considerably less. It increases when we move from NF to FF.

Table 7
Projected future maximum temperature [°C] at Chamelia watershed based on ensemble of five RCMs under RCP scenarios.

Change from baseline [°C]			DJF	MAM	JJAS	ON	Annual
Baseline [°C]			18.0	26.9	28.5	24.1	24.8
RCP 4.5	NF	Mean [°C]	1.2	0.8	0.7	0.8	0.9
		Range [°C]	0.2–3.4	−0.4–2.1	0.1–1.3	0.3–2.0	0.4–1.7
	MF	Mean [°C]	1.7	1.5	1.1	1.1	1.4
		Range [°C]	0.6–2.7	0.1–3.0	0.5–1.9	0.2–2.2	0.8–1.8
	FF	Mean [°C]	2.2	1.6	1.3	1.5	1.6
		Range [°C]	0.8–3.3	0.6–2.7	0.5–2.3	0.7–2.5	1.1–2.0
RCP 8.5	NF	Mean [°C]	1.4	1.2	0.8	0.9	1.1
		Range [°C]	0.4–2.6	−0.3–2.2	0.2–1.5	0.4–2.2	0.3–1.7
	MF	Mean [°C]	2.8	2.2	1.5	2.0	2.1
		Range [°C]	1.6–3.7	0.6–3.2	0.6–2.3	0.7–2.8	1.0–2.9
	FF	Mean [°C]	4.3	3.5	2.6	3.4	3.4
		Range [°C]	3.0–6.1	2.5–4.5	1.5–3.4	2.4–4.7	2.6–4.2

3.4. Climate change impacts on water availability

Change in water balance components under he projected changes in future temperature and precipitation were simulated using the calibrated and validated SWAT model and analysed at annual as well as seasonal scales. The water balance components considered were:

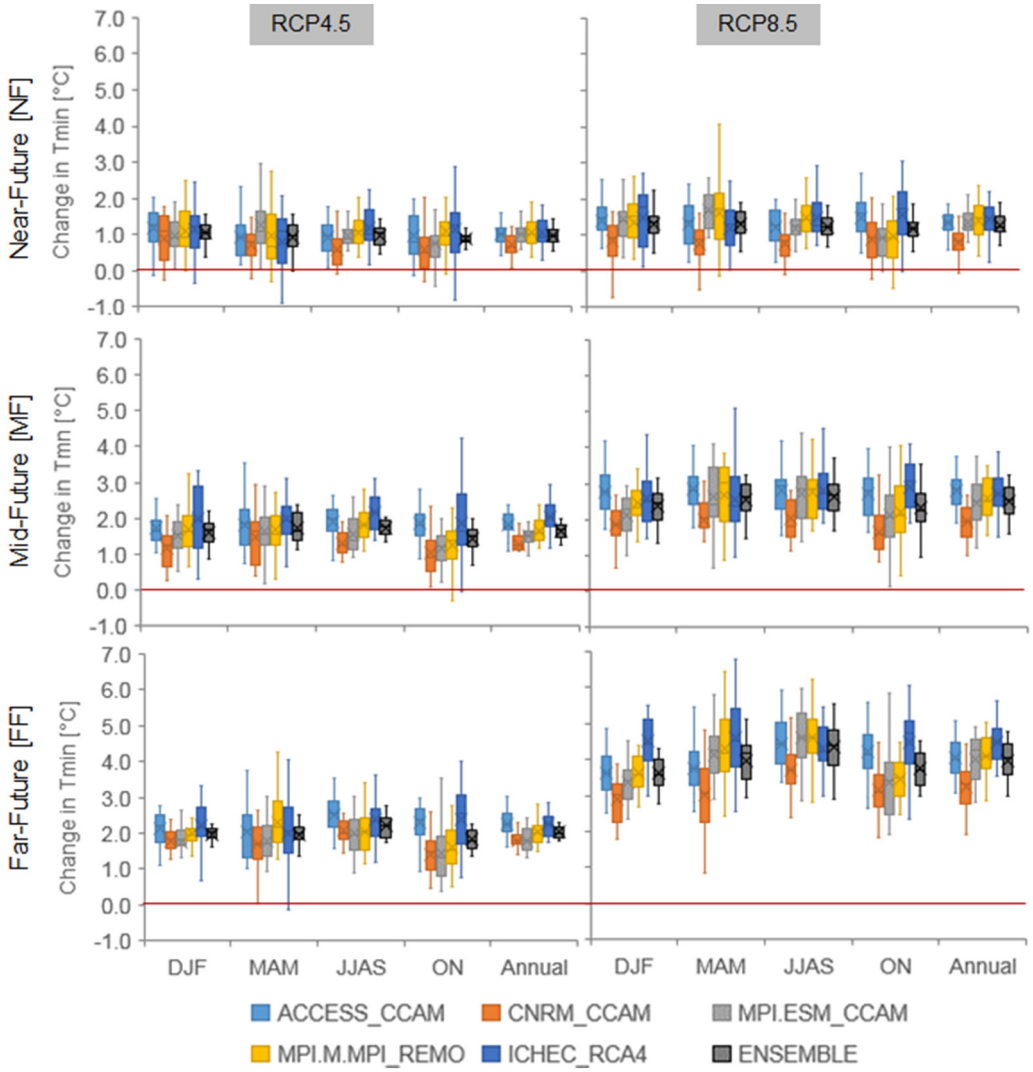

Fig. 12. Range of projected change in future minimum temperature for different scenarios and RCMs for the study watershed. Each box represents range in one RCM where whiskers indicate max and min values excluding the outliers, line markers indicate the median and x markers indicate the mean of change in annual total precipitation projected for each future timeframe.

precipitation, snowmelt, evapotranspiration, and water yield. Since observed data for all the water balance components for the basin was not available, we used the SWAT output for current hydrology as the reference baseline to estimate changes in the water balance components for future scenarios. Climate change impacts are assessed at Qt120 (sub-basin ID: 13) located near to the outlet of the Chamelia (Fig. 1).

Table 8
Projected future minimum temperature [°C] at Chamelia watershed based on ensemble of five RCMs under RCP scenarios.

Change from baseline [°C]			DJF	MAM	JJAS	ON	Annual
Baseline [°C]			5.1	13.3	19.2	11.1	12.9
RCP 4.5	NF	Mean [°C]	1.1	0.9	1.0	0.9	0.9
		Range [°C]	0.4–1.6	0–1.6	0.5–1.4	0.4–1.7	0.5–1.4
	MF	Mean [°C]	1.6	1.7	1.8	1.4	1.6
		Range [°C]	0.9–2.2	1.1–2.4	1.3–2.1	0.7–2	1.2–1.9
	FF	Mean [°C]	2.0	2.0	2.2	1.8	2.0
		Range [°C]	1.1–2.3	0.8–2.7	1.7–2.8	1.4–2.3	1.7–2.3
RCP 8.5	NF	Mean [°C]	1.3	1.3	1.2	1.2	1.2
		Range [°C]	0.5–2.3	0.5–1.9	0.7–1.8	0.4–2.4	0.7–1.9
	MF	Mean [°C]	2.4	2.5	2.6	2.3	2.5
		Range [°C]	1.4–3.1	1.5–3.2	1.7–3.7	1–3.6	1.6–3.2
	FF	Mean [°C]	3.6	4.0	4.3	3.7	3.9
		Range [°C]	2.8–4.3	2.9–5.1	2.9–5.6	3–4.5	2.9–4.7

The projected range of streamflow change for the future periods, scenarios, and RCMs are shown in Fig. 13. The projected change in streamflow for an ensemble of five RCMs shows increasing trend for annual as well as seasonal values, for all the future periods considered, and for all the scenarios. For reasons other than MAM, individual RCMs project increase in future streamflow with means and medians lying above zero. As was seen for projected precipitation in Fig. 10, REMO projections are relatively dry while ICHEC_RCA4 projections are wetter than other RCMs. ICHEC_RCA4 also has the widest range of streamflows.

Average annual streamflow is projected to increase gradually from NF towards MF under both the scenarios (Fig. 14). For RCP4.5, the annual values are projected to increase by 8.2% in NF, 12.2% in MF, and 15.0% in FF. Such a significant increase was also reported for other watersheds in Nepal (e.g., Immerzeel et al., 2013; Bhattarai and Regmi, 2016). The projected increasing trend is consistent across all the seasons (Fig. 14). However, the increase in streamflow is greater in winter (DJF), and then for pre-monsoon (MAM), post-monsoon (ON), and then to monsoon (JJAS) seasons. Considering RCP4.5 scenarios, the projected increase in winter season (DJF) flow is 34% in NF, 40% in MF, and 42% in FF. In addition, uncertainties in the simulate flow are shown with a grey

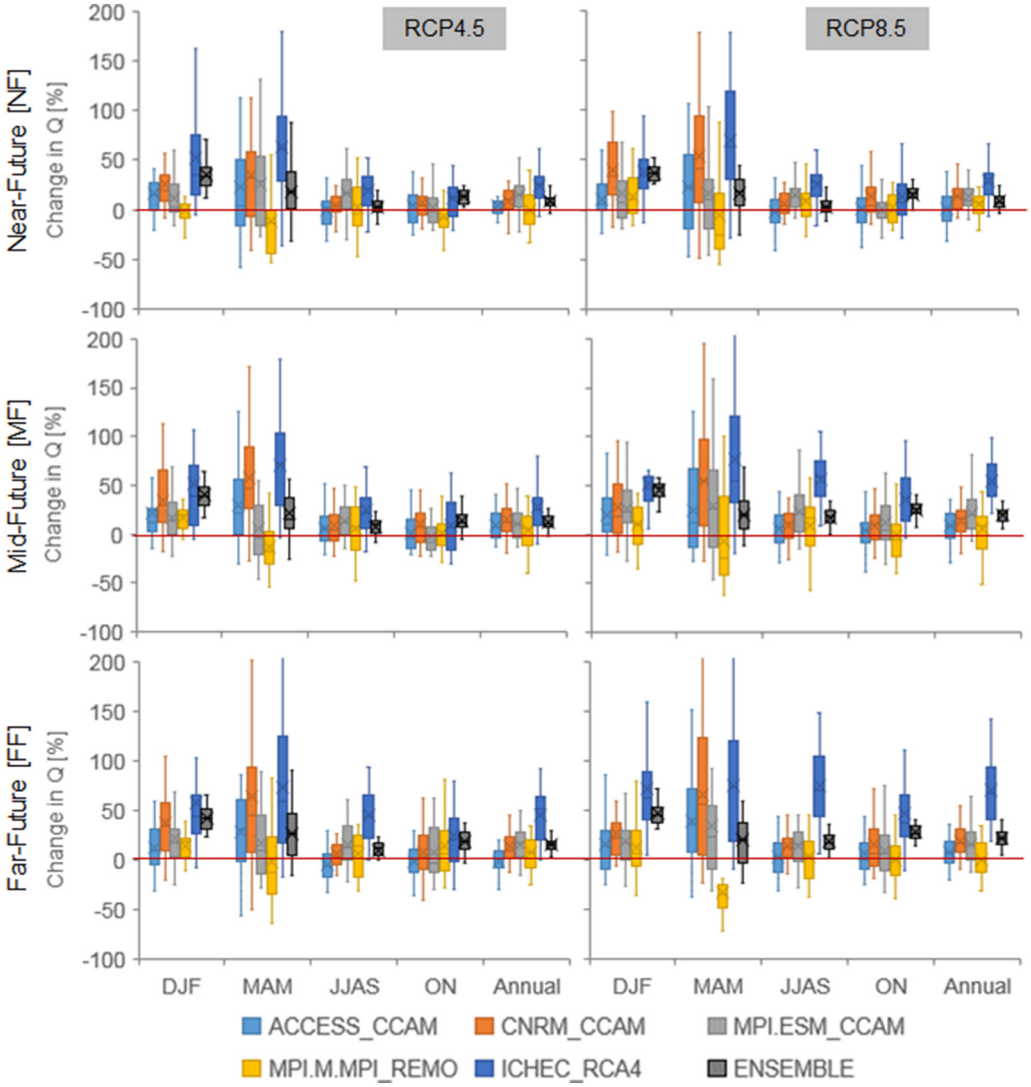

Fig. 13. Range of projected change (%) in simulated streamflow for the future periods, scenarios, and RCMs in the Chamelia watershed. Each box represents range in one RCM where whiskers indicate max and min values excluding the outliers, line markers indicate the median and x markers indicate the mean of change in annual total precipitation projected for each future timeframe.

band indicating minimum-maximum range in projections as well as average values for each period future timeframe. For long-term average flow, historical as well as projected flows for all the seasons lie within the mix-max band. The bandwidth is wider during high-flow season and gradually decreases during low flow seasons. The wider bandwidth indicating higher model prediction uncertainty may be propagated by natural variability observed in streams during the high flow periods. Similar trends can be seen in the historical and projected FDC shown in the third row of Fig. 14.

Fig. 15 further analyses the change in water balance components under future scenarios. The net water yield here refers to the net amount of water contributed by the sub-basins and HRUs to the streamflow. The increase in streamflow is mostly contributed by increases in precipitation (Fig. 15). The increase in total streamflow is less compared to the increase in precipitation because of loss of some precipitation by evapotranspiration. In addition, percolation has also increased significantly with an increasing rate towards the future (e.g., 37.1% in NF, 40.1% in MF, and 43.7% in FF under RCP4.5 scenario). On the other hand, even though the precipitation and total streamflow have increased, overland flow (SurQ) has decreased. In Annex-4 we further analysed changes in actual evapotranspiration (AET) to confirm the trend. Figures show that AET is projected to increase from near to far future across all the months/seasons and scenarios as the result of projected increase in temperature. The projected increase (w.r.t. baseline) in average annual AET for RCP8.5 scenario ranges from 15% in NF to 20% in FF; however, there is a strong seasonality in magnitude of the change. The increase in DJF season ranges from 58% (NF) to 68% (FF), whereas from 29% (NF) to 37% (FF) (Annex-4). The aforementioned results indicate that more of SURQ is projected to be lost as AET and there is a likelihood of an increase in groundwater recharge with increased precipitation, and subsequent release into streams in the form of baseflow (lateral flow and groundwater flow). The most affected water balance component in the Chamelia watershed is the percolation (with the largest percentage increase) followed by net water yield, AET, and precipitation. The increased precipitation may result increased frequency of wet soil conditions that are conducive to percolation.

4. Conclusions

SWAT model was developed to simulate hydrological responses of the Chamelia watershed. The model performance is reasonably good in terms of capability to reproduce hydrological patterns including flow duration curves and statistical properties of the observed daily

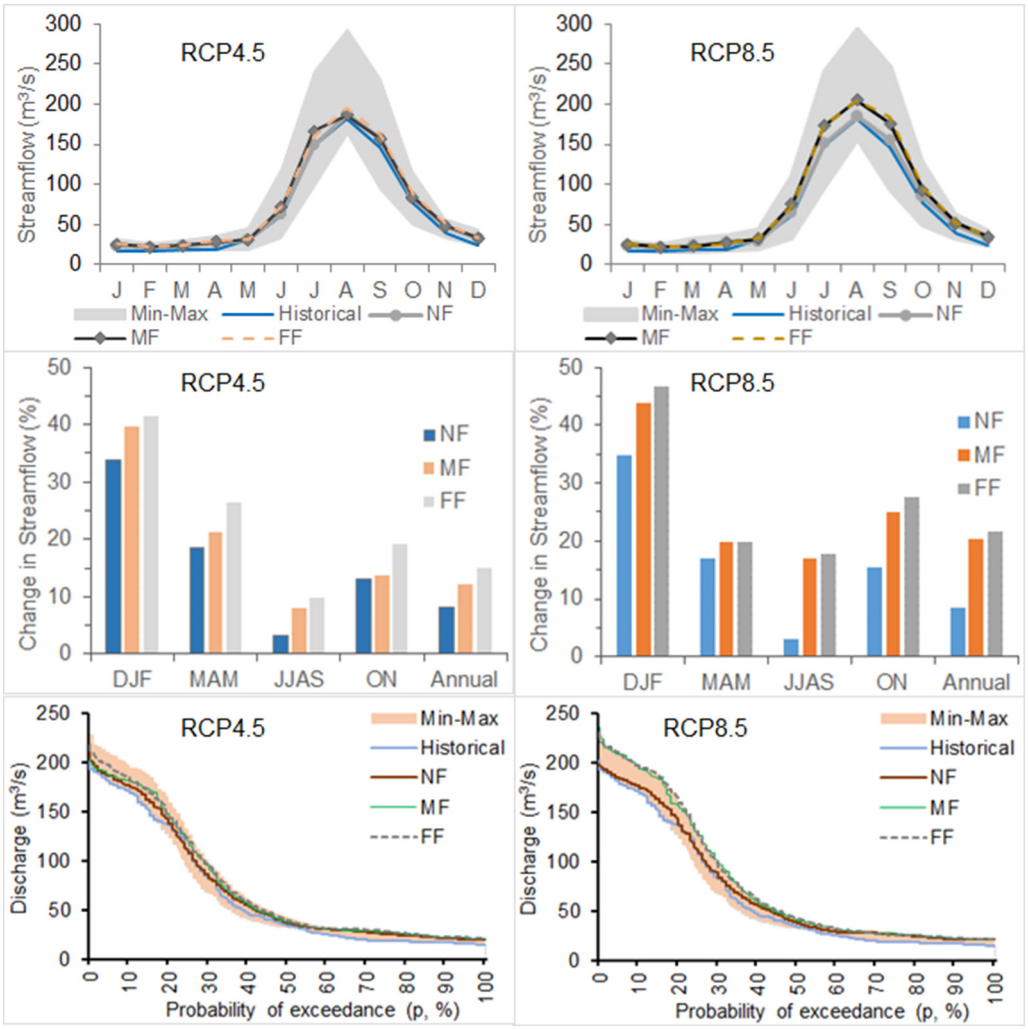

Fig. 14. Change in simulated streamflow at Q120 station under future climate represented as an ensemble of selected RCM outputs for RCP4.5 (top) and RCP8.5 (bottom) scenarios. The first, second and third rows show monthly hydrograph, change in streamflow from baseline, and flow duration curve (FDC), respectively. NF, MF and FF refer to near-, mid- and far-futures, respectively; Min-Max refer to a band of variation for the months.

and monthly time-series. Multi-site calibration approach has ensured better representation of hydrological variability within the sub-basin. The model is most reliable for Q120 along the main stem of the watershed, which is also the most important station from a hydropower development perspective.

Future climatic conditions were taken from five RCMs under two RCP scenarios and bias corrected using quantile mapping method. On an average, both annual and seasonal values of precipitation are projected to increase, with a greater percentage of increase in winter and pre-monsoon seasons. However, models project both increases

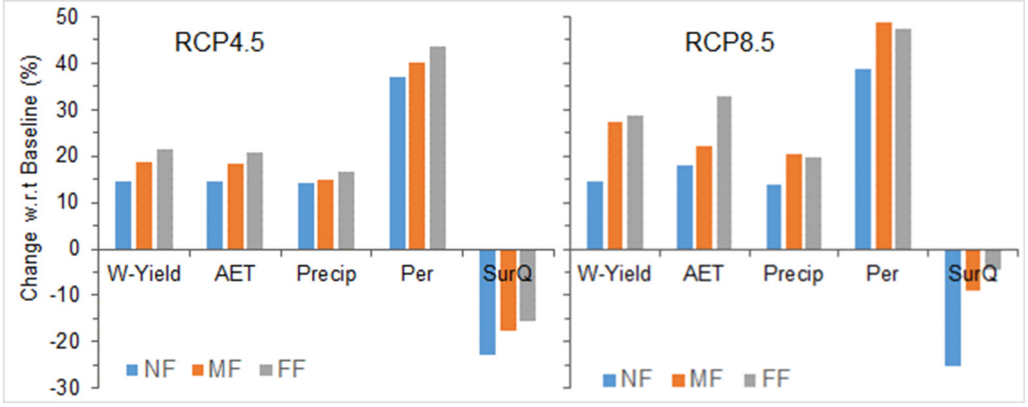

Fig. 15. Impacts of projected changes in precipitation and temperature on annual average water balance components in the Chamelia watershed for near future (NF), mid future (MF), and far future (FF) under RCP4.5 and RCP8.5 scenarios. W-Yield is water yield; AET is actual evapotranspiration; Precip is precipitation; Snow is snowmelt; Per is percolation; and SurQ is surface runoff (or overland flow).

and decreases in precipitation over the years, indicating lack of consensus about precipitation change. Both maximum and minimum temperatures are projected to increase with higher certainty than with precipitation; albeit, with varying rates. Water availability in the changed future climate is also projected to increase gradually from baseline to near-, mid-, and far-futures. An ensemble of five RCMs shows dry season (or pre-monsoon and winter) water availability is projected to increase at a higher rate than the average annual values, which would be beneficial for water resources infrastructure projects.

While the average values for future precipitation, temperature and streamflow indicate increases across all parameters for all the futures, the SWAT model and RCMs considered also project decreases in these values over time. Especially when looking at seasonal responses, precipitation does not have a generic trend across the seasons. Based on the five RCMs considered here across all futures for RCP 4.5, average annual changes in precipitation at st103 may vary between −10 and 34%; maximum temperature between 0.4 and 2.0 °C; and minimum temperature between 0.5 and 2.3 °C. A deeper look at the consensus seen across the models in each season is needed to further quantify the likelihood of values within these ranges of projected future climate and water resource availability.

Local watersheds might also have various projects of importance even if the sizes are not that large. This study indicates that local watersheds could be vulnerable to climatic risks and therefore should be considered in the planning process. Results from this study provide a benchmark for water available in the basin and discussion of water allocation and use across various water users in the basin. Especially with discussions of hydropower development, the quantification of water balance components will be a key information for understanding impacts across the water-energy-food nexus. Furthermore, as downstream watersheds have more base flow, interventions in the form of recharge or watershed protection in the upstream is likely to have positive impact in terms of enhancing dry season flows in the downstream. Therefore, water management needs to be coordinated across the basin.

Acknowledgements

This study is made possible by the generous support of the American people through the United States Agency for International Development (USAID) under Digo Jal Bikas (DJB) project. The contents are the responsibility of the authors and do not necessarily reflect the views of USAID or the United States Government. We would like to acknowledge Miss. Claire Swingle for her help in language editing.

Appendix A. Supplementary data

Supplementary data to this article can be found online at https://doi.org/10.1016/j.scitotenv.2018.09.053.

References

Abbaspour, K.C., et al., 2007. Modelling hydrology and water quality in the pre-alpine/alpine Thur watershed using SWAT. J. Hydrol. 333 (2–4), 413–430.
Allen, R.G., Pereira, L.S., Raes, D., Smith, M., 1998. Meteorological data – radiation. Crop Evapotranspiration - Guidelines for Computing Crop Water Requirements. FAO Irrigation and Drainage Paper 56. Food and Agriculture Organization (FAO), Rome, Italy.
Andermann, C., Longuevergne, L., Bonnet, S., Crave, A., Davy, P., Gloaguen, R., 2012. Impact of transient groundwater storage on the discharge of Himalayan rivers. Nat. Geosci. 5, 127–132.
Arnold, J.G., Srinivasan, P., Muttiah, R.S., Williams, J.R., 1998. Large area hydrologic modelling and assessment. Part I. Model development. J. Am. Water Resour. Assoc. 34, 73–89.
Arnold, J.G., Moriasi, D.N., Gassman, P.W., Abbaspour, K.C., White, M.J., Srinivasan, R., Santhi, C., Harmel, R.D., Van Griensven, A., Van Liew, M.W., Kannan, N., Jha, M.K., 2012. SWAT: model use, calibration, and validation. Trans. Am. Soc. Agric. Biol. Eng. (ASABE) 55 (4), 1491–1508.
Bajracharya, A.R., Bajracharya, S.R., Shrestha, A.B., Maharjan, S.B., 2018. Climate change impact assessment on the hydrological regime of the Kaligandaki Basin, Nepal. Sci. Total Environ. 625, 837–848.
Barnett, T.P., Adam, J.C., Lettenmaier, D.P., 2005. Potential impacts of a warming climate on water availability in snow-dominant regions. Nature 438, 303–309.
Bates, B.C., Kundzewicz, Z.W., Wu, S., Palutikof, J.P. (Eds.), 2008. Climate Change and Water: Technical Paper of the Intergovernmental Panel on Climate Change (IPCC). IPCC Secretariat, Geneva (210 pp.).
Berg, P., Feldmann, H., Panitz, H.J., 2012. Bias correction of high resolution regional climate model data. J. Hydrol. 448–449, 80–92.
Bharati, L., Gurung, P., Jayakody, P., Smakhtin, V., Bhattarai, U., 2014. The projected impact of climate change on water availability and development in the Koshi Basin, Nepal. Mt. Res. Dev. 34, 118–130.
Bharati, L., Gurung, P., Maharjan, L., Bhattarai, U., 2016. Past and future variability in the hydrological regime of the Koshi Basin, Nepal. Hydrol. Sci. J. 61 (1), 79–93.
Bhattarai, B.C., Regmi, D., 2016. Impact of climate change on water resources in view of contribution of runoff components in stream flow: a case study from Langtang Basin, Nepal. J. Hydrol. Meteorol. 9 (1), 74–84.
Bolch, T., Kulkarni, A., Kääb, A., Huggel, C., Paul, F., Cogley, J.G., ... Bajracharya, S., 2012. The state and fate of Himalayan glaciers. Science 336 (6079), 310–314.
Chen, J., Brissette, F.P., Chaumont, D., Braun, M., 2013. Finding appropriate bias correction methods in downscaling precipitation for hydrologic impact studies over North America. Water Resour. Res. 49, 4187–4205.
Choudhary, A., Dimri, A.P., 2017. Assessment of CORDEX-South Asia experiments for monsoonal precipitation over Himalayan region for future climate. Clim. Dyn. 1–22.
Devkota, L.P., Gyawali, D.R., 2015. Impacts of climate change on hydrological regime and water resources management of the Koshi River Basin, Nepal. J. Hydrol. Reg. Stud. 4 (Part B), 502–515.
Dijkshoorn, J.A., Huting, J.R.M., 2009. Soil and Terrain (SOTER) Database for Nepal. Report 2009/01. ISRIC – World Soil Information, Wageningen Available at. http://www.isric.org/isric/webdocs/docs/ISRIC_Report_2009_01.pdf, Accessed date: 15 December 2016 (Online Dataset).
Dixit, A., Upadhya, M., Dixit, K., Pokhrel, A., Rai, D.R., 2009. Living With Water Stress in the Hills of the Koshi Baisn, Nepal. ICIMOD, Nepal.
Fontaine, T.A., Cruickshank, T.S., Arnold, J.G., Hotchkiss, R.H., 2002. Development of a snowfall–snowmelt routine for mountainous terrain for the soil water assessment tool (SWAT). J. Hydrol. 262 (1), 209–223.
Ghimire, S., Choudhary, A., Dimri, A.P., 2015. Assessment of the performance of CORDEX-South Asia experiments for monsoonal precipitation over the Himalayan region during present climate: part I. Clim. Dyn. 2–4.
Gudmundsson, L., Bremnes, J.B., Haugen, J.E., Engen-Skaugen, T., 2012. Technical note: downscaling RCM precipitation to the station scale using statistical transformations — a comparison of methods. Hydrol. Earth Syst. Sci. 16, 3383–3390.
Gupta, H.V., Sorooshian, S., Yapo, P.O., 1999. Status of automatic calibration for hydrologic models: comparison with multilevel expert calibration. J. Hydrol. Eng. 4 (2), 135–143.
Hasan, M.A., Pradhanang, S.M., 2017. Estimation of flow regime for a spatially varied Himalayan watershed using improved multi-site calibration of the Soil and Water Assessment Tool (SWAT) model. Environ. Earth Sci. 76 (23), 787. https://doi.org/10.1007/s12665-017-7134-3.
ICIMOD, 2010. Land Cover of Nepal 2010. International Center for Integrated Mountain Development (ICIMOD), Kathmandu, Nepal Available online at:. http://rds.icimod.org/Home/DataDetail?metadataId=9224, Accessed date: 12 January 2017.
Immerzeel, W.W., Pellicciotti, F., Bierkens, M.F.P., 2013. Rising river flows throughout the twenty-first century in two Himalayan glacierized watersheds. Nat. Geosci. 6, 742–745.
IPCC, 2013. In: Stocker, T.F., Qin, D., Plattner, G.K., Tignor, M.M.B., Allen, S.K., Boschung, J., Nauels, A., Xia, Y., Bex, V., Midgley, P.M. (Eds.), Climate Change 2013: The Physical Science Basis. Intergovernmental Panel on Climate Change, Working Group I Contribution to the IPCC Fifth Assessment Report (AR5). Cambridge Univ Press, New York.
IWMI, 2014. Water Availability and Agricultural Adaptation Options of the Koshi Basin Under Global Environmental Change. Final Report Submitted by International Water Management Institute (IWMI) to International Center for Integrated Mountain Development (ICIMOD), December 2014 (Kathmandu).
IWMI, 2017. Progress Report of Digo Jal Bikas (DJB) Project Submitted to United States Agency for International Development (USAID). International Water Management Institute (IWMI), Kathmandu, Nepal (September, 2017).
Khadka, D., Babel, M.S., Shrestha, S., Tripathi, N.K., 2014. Climate change impact on glacier and snow melt and runoff in Tamakoshi basin in the Hindu Kush Himalayan (HKH) region. J. Hydrol. 511, 49–60.
Kim, U., Kaluarachchi, J.J., 2009. Climate change impacts on water resources in the Upper Blue Nile river basin, Ethiopia. J. Am. Water Resour. Assoc. 45 (6), 1361–1378.
Knutti, R., Furrer, R., Tebaldi, C., Cermak, J., Meehl, G.A., 2010a. Challenges in combining projections from multiple climate models. J. Clim. 23, 2739–2758.
Knutti, R., Abramowitz, G., Collins, M., Eyring, V., Gleckler, P.J., Hewitson, B., Mearns, L., 2010b. Good practice guidance paper on assessing and combining multi model climate projections. IPCC Expert Meet. Assess. Comb. Multi Model Clim. Proj. (15 pp.)
Krishnan, N., Raj, C., Chaubey, I., Sudheer, K.P., 2018. Parameter estimation of SWAT and quantification of consequent confidence bands of model simulations. Environ. Earth Sci. 77 (12), 470. https://doi.org/10.1007/s12665-018-7619-8.
Kure, S., Jang, S., Ohara, N., Kavvas, M.L., Chen, Z.Q., 2013. Hydrological impact of regional climate change for the snowfed and glacierfed river basins in the Republic of Tajikistan: hydrological responses of flow to climate change. Hydrol. Process. 27 (26), 4057–4070.
Latif, M., 2011. Uncertainty in climate change projections. J. Geochem. Explor. 110 (1), 1–7.
Leta, O.T., et al., 2015. Assessment of the different sources of uncertainty in a SWAT model of the River Senne (Belgium). Environ. Model. Softw. 68, 129–146.
Li, H., Xu, C.Y., Beldring, S., Tallaksen, L.M., Jain, S.K., 2016. Water resources under climate change in Himalayan basins. Water Resour. Manag. 30 (2), 843–859.

Liu, Y.B., de Smedt, F., 2004. WetSpa Extension, a GIS-based Hydrologic Model for Flood Prediction and Watershed Management – Documentation and User Manual. Department of Hydrology and Hydraulic Engineering, Vrije Universiteit Brussel, Brussel, Belgium, pp. 1–126.

Lutz, A.F., ter Maat, H.W., Biemans, H., Shrestha, A.B., Wester, P., Immerzeel, W.W., 2016. Selecting representative climate models for climate change impact studies: an advanced envelope-based selection approach. Int. J. Climatol. 36, 3988–4005.

Manandhar, S., Pandey, V.P., Ishidaira, H., Kazama, F., 2013. Perturbation study of climate change impacts in a snow-fed river basin. Hydrol. Process. 27, 3461–3474.

McGregor, J.L., Dix, M.R., 2001. The CSIRO Conformal-Cubic Atmospheric GCM. In: Hodnett, P.F. (Ed.), IUTAM Symposium on Advances in Mathematical Modelling of Atmosphere and Ocean Dynamics. Fluid Mechanics and Its Applications vol. 61. Springer, Dordrecht.

Moriasi, D.N., Arnold, J.G., van Liew, M.W., Bingner, R.L., Harmel, R.D., Veith, T.L., 2007. Model evaluation guidelines for systematic quantification of accuracy in watershed simulations. Trans. ASABE 50 (3), 885–900.

Mukherjee, S., Hazra, A., Kumar, K., Nandi, S.K., Dhyani, P.P., 2017. Simulated projection of ISMR over Indian Himalayan region: assessment from CSIRO-CORDEX South Asia experiments. Meteorog. Atmos. Phys. 1–17.

NASA JPL, 2009. Advanced Spaceborne Thermal Emission and Reflection Radiometer (ASTER) Global Digital Elevation Model Version 2 (GDEM V2). United States National Aeronautics and Space Administration – Jet Propulsion Laboratory (NASA JPL) https://doi.org/10.5067/ASTER/ASTGTM.002 (accessed on March 27, 2013).

Nash, J.E., Sutcliffe, J.V., 1970. River flow forecasting through conceptual models part I – a discussion of principles. J. Hydrol. 10 (3), 282–290.

Neitsch, S., Arnold, J., Kiniry, J., Williams, J., 2011. Soil and Water Assessment Tool Theoretical Documentation Version 2009. Texas Water Resources Institute, Texas A&M University System, Texas.

Rahman, K., Marinanti, C., Beniston, M., Widmer, F., Abbaspour, K., Lehmann, A., 2012. Streamflow modeling in a highly managed mountainous glacier watershed using SWAT: the Upper Rhone River watershed case in Switzerland. Water Resour. Manag. 27 (2), 323–339.

Rasul, G., 2016. Managing the food, water, and energy nexus for achieving the sustainable development goals in South Asia. Environ. Dev. 18, 14–25.

Rostamian, R., Jaleh, A., Afyuni, M., Mousavi, S.F., Heidarpour, M., Jalalian, A., Abbaspour, K.C., 2008. Application of a SWAT model for estimating runoff and sediment in two mountainous basins in central Iran. Hydrol. Sci. J. 53 (5), 977–988.

Saeed, F., Suleri, A.Q., 2015. Future Heat Waves in Pakistan Under IPCCs AR5 Climate Change Scenario. Sustainable Development Policy Institute, Islamabad, Pakistan.

Saltelli, A., Ratto, M., Tarantola, S., Campolongo, F., 2006. Sensitivity analysis practices: strategies for model-based inference. Reliab. Eng. Syst. Saf. 91, 1109–1125.

Samuelsson, P., Jones, C.G., Willen, U., Ullerstig, A., Gollvik, S., Hansson, U., Jansson, C., Ejellstrom, E., Nikulin, G., Wyser, K., 2011. The Rossby Centre regional climate model RCA3: model description and performance. Tellus 63 (1), 4–23.

Sanjay, J., Krishnan, R., Shrestha, A.B., Rajbhandari, R., Ren, G.Y., 2017. Downscaled climate change projections for the Hindu Kush Himalayan region using CORDEX South Asia regional climate models. Adv. Clim. Chang. Res. 8, 185–198.

Scinocca, J.F., et al., 2015. Coordinated global and regional climate modeling. J. Clim. 29 (1), 17–35.

Shrestha, S., Htut, A.Y., 2016. Modeling the potential impacts of climate change on hydrology of the Bago River Basin, Myanmar. Int. J. River Basin Manag. 14 (3), 287–297.

Shrestha, M., Acharya, S.C., Shrestha, P.K., 2017a. Bias correction of climate models for hydrological modelling – are simple methods still useful? Meteorol. Appl. https://doi.org/10.1002/met.1655 (xx: xx-xx).

Shrestha, N.K., Du, X., Wang, J., 2017b. Assessing climate change impacts on fresh water resources of the Athabsca River Basin, Canada. Sci. Total Environ. 601–602, 425–440.

Siddiqui, S., Bharati, L., Gurung, P., Maharjan, L.D., 2012. Climate Change and Vulnerability Mapping in Watersheds in Middle and High Mountains of Nepal. International Water Management Institute (IWMI), Kathmandu, Nepal.

Srinivasan, R., 2012. Beginner SWAT - Training Manual.

Srinivasan, R., Ramanarayanan, T.S., Arnold, J.G., Bednarz, S.T., 1998. Large area hydrological modeling and assessment. Part II: model application. J. Am. Water Resour. Assoc. 34 (1), 91–101.

Teichmann, C., Eggert, B., Elizalde, A., Haensler, A., Jacob, D., Kumar, P., Moseley, C., Pfeifer, S., Rechid, D., Remedio, A., Ries, H., Petersen, J., Preuschmann, S., Raub, T., Saeed, F., Sieck, K., Weber, T., 2013. How does a regional climate model modify the projected climate change signal of the driving GCM: a study over different CORDEX regions using REMO. Atmosphere 4 (2), 214–236.

Teutschbein, C., Seibert, J., 2012. Bias correction of regional climate model simulations for hydrological climate-change impact studies: review and evaluation of different methods. J. Hydrol. 456–457, 12–29.

ul Hasson, S., 2016. Seasonality of precipitation over himalayan watersheds in CORDEX South Asia and their driving CMIP5 experiments. Atmosphere (Basel) 7, 123.

Van Vuuren, D.P., Edmonds, J., Kainuma, M., Riahi, K., Thomson, A., Hibbard, K., Hurtt, G.C., Kram, T., Krey, V., Lamarque, J.F., Masui, T., Meinshausen, M., Nakicenovic, N., Smith, S.J., Rose, S.K., 2011. The representative concentration pathways: an overview. Clim. Chang. 109, 5–31.

Versini, P.A., Pouget, L., McEnnis, S., Custodio, E., Escaler, I., 2016. Climate change impact on water resources availability: case study of the Llobregat river basin (Spain). Hydrol. Sci. J. 61 (14), 2496–2508.

WECS, 2011. Water Resources of Nepal in the Context of Climate Change. Water and Energy Commission Secretariat (WECS), Government of Nepal, Kathmandu.

Wilby, R.L., 2010. Evaluating climate model outputs for hydrological applications. Hydrol. Sci. J. 55, 1090–1093.

Wood, A.W., Leung, L.R., Sridhar, V., Lettenmaier, D.P., 2004. Hydrologic implications of dynamical and statistical approaches to downscaling climate model outputs. Climate Change 62, 189–216.

World Bank, 2009. Glacier Retreat in the Nepal Himalaya: An Assessment of the Role of Glaciers in the Hydrologic Regime of the Nepal Himalaya. Prepared for the South Asia Sustainable Development (SASDN) Office, Environment and Water Resources Unit.

Zhu, T., Ringler, C., 2012. Climate change impacts on water availability and use in the Limpopo river basin. Water 4, 63–84.